

## Targeted Polymersome Delivery of siRNA Induces Cell Death of Breast Cancer Cells Dependent upon Orai3 Protein Expression

Todd O. Pangburn, Katerina Georgiou, Frank S. Bates, and Efrosini Kokkoli\*

Department of Chemical Engineering and Materials Science, University of Minnesota, Minneapolis, Minnesota 55455, United States

**ABSTRACT:** Polymersomes, polymeric vesicles that self-assemble in aqueous solutions from block copolymers, have been avidly investigated in recent years as potential drug delivery agents. Past work has highlighted peptide-functionalized polymersomes as a highly promising targeted delivery system. However, few reports have investigated the ability of polymersomes to operate as gene delivery agents. In this study, we report on the encapsulation and delivery of siRNA inside of peptide-functionalized polymersomes composed of poly(1,2-butadiene)-*b*-poly(ethylene oxide). In particular, PR\_b peptide-functionalized polymer vesicles are shown to be a promising system for siRNA delivery. PR\_b is a fibronectin mimetic peptide targeting specifically the  $\alpha_5\beta_1$  integrin. The Orai3 gene was targeted for siRNA knockdown, and PR\_b-functionalized polymer vesicles encapsulating siRNA were found to specifically decrease cell viability of T47D breast cancer cells to a certain extent, while preserving viability of noncancerous MCF10A breast cells. siRNA delivery by PR\_b-functionalized polymer vesicles was compared to that of a current commercial siRNA transfection agent, and produced less dramatic decreases in cancer cell viability, but compared favorably in regards to the relative toxicity of the delivery systems. Finally, delivery and vesicle release of a fluorescent encapsulate by PR\_b-functionalized polymer vesicles was visualized by confocal microscopy, and colocalization with cellular endosomes and lysosomes was assessed by organelle staining. Polymersomes were observed to primarily release their encapsulate in the early endosomal intracellular compartments, and data may suggest some escape to the cytosol. These results represent a promising first generation model system for targeted delivery of siRNA.



### INTRODUCTION

Small interfering RNA (siRNA), discovered only a decade ago, has rapidly been applied as both a tool for profiling protein function and a potential therapeutic for a wide array of diseases.<sup>1–3</sup> siRNA molecules, double-stranded RNA typically 20–25 nucleotides in length, act to down-regulate expression of a specific target gene. This down-regulation is accomplished with help from the cell's own RNA interference machinery. A single strand of the siRNA molecule is selected by the cell, typically the antisense strand, and incorporated into an endogenous RISC (RNA-induced silencing complexes) assembly in the cytosol, which then acts to catalytically degrade complementary messenger RNA (mRNA).<sup>4</sup> Of interest to this work, a number of gene targets have been identified with potential relevance for the treatment of cancer.<sup>5</sup> In particular, the calcium channel protein, Orai3, has been recently identified as a potential therapeutic target for breast cancer.<sup>6</sup>

Down-regulation of Orai3 in breast cancer cells was found to reduce cell viability of T47D human breast cancer cells and arrest cell cycle in the G1 phase eventually leading to apoptosis, while for noncancerous MCF10A breast cells down-regulation of Orai3 resulted in no measurable decrease in cell viability.<sup>6</sup> Thus, Orai3 was identified as a potential breast cancer-specific therapeutic target for siRNA down-regulation. Orai3 is one of a class of calcium channel proteins located on the plasma membrane (along with Orai1 and 2) that operates along with the stromal interacting molecule (STIM) proteins to replenish calcium levels within the cell via what is termed the store operated calcium ( $\text{Ca}^{2+}$ ) entry (SOCE) pathway.<sup>7,8</sup> The SOCE

pathway is ubiquitous and has been shown to be important for a number of cell functions including cell cycle progression, cell proliferation, and migration.<sup>9–11</sup> In addition, there is evidence that SOCE is mediated by Orai3 in many breast cancer cells, as opposed to being dominated by the canonical Orai1-mediated pathway observed in noncancerous cells.<sup>12–14</sup> It has been proposed that the dominance of either Orai1 or Orai3 in the SOCE pathway is dependent upon which is rate limiting under the particular conditions of the cell.<sup>15</sup> Moreover, Orai3 was found to be overexpressed in the majority of breast cancer tumors tested as compared to noncancerous tissue in the same patient.<sup>6</sup> Considering this current body of evidence, Orai3 was chosen as a potential cancer-specific target for siRNA delivery to breast cancer cells.

Effective delivery of siRNA molecules to tumors and cancer cells presents a number of unique challenges.<sup>16,17</sup> First, RNA is rapidly degraded in the presence of serum or really any ribonuclease (RNase), so that for effective delivery the siRNA molecules must be protected from degradation.<sup>18,19</sup> Second, because siRNA is a highly negatively charged and relatively large molecule (~13 kDa), it cannot effectively gain entry into a cell alone, and intracellular delivery must typically be assisted. Finally, siRNA has to get specifically to the cytosol of the cell to assemble with the RISC protein complex, which in most cases means that the siRNA must escape the endosomal and

Received: February 29, 2012

Revised: June 11, 2012

Published: July 24, 2012

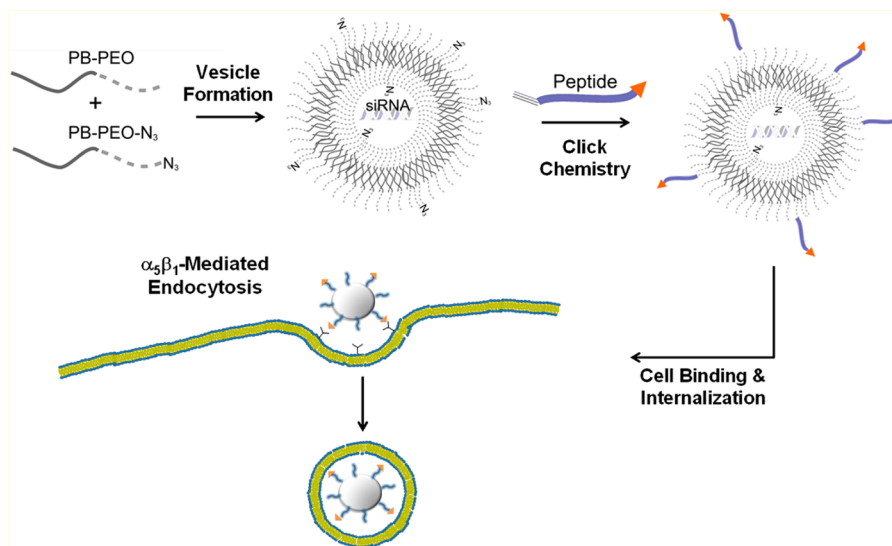


**Figure 1.** Schematic representation of vesicle formation, peptide conjugation of PB-PEO (OB) polymer vesicles, and interaction with cells.

lysosomal intracellular compartments. All of these barriers to delivery exist for both *in vitro* and *in vivo* siRNA delivery; however, additional challenges present themselves for the case of *in vivo* delivery, including finding and delivery to the appropriate tissue in the body, evading host immune response and phagocytosis, colloidal stability, toxicity, and avoiding simple filtration in the kidneys.<sup>17</sup> We expected that cancer targeting peptide-functionalized polymersomes could be a facile delivery agent of siRNA, well poised to confront the challenges of siRNA delivery, and tested that expectation in this work with model polymersomes. It should be noted that, although the current work tests strictly the *in vitro* efficacy of our model siRNA delivery system, the findings presented here could be extended to biodegradable polymersome systems, which have been shown to be well suited to overcome the challenges of *in vivo* delivery.<sup>20</sup>

Polymersomes are essentially polymeric nanocapsules similar in construction and function to their low molecular weight analogues, liposomes.<sup>21,22</sup> They are self-assembled structures formed from amphiphilic block copolymers in aqueous solution. For example, the diblock copolymer, poly(1,2-butadiene)-*b*-poly(ethylene oxide) (PB-PEO or OB), used in this study self-assembles to form thick polymer membranes composed of a PB membrane core with PEO brush layers shielding this hydrophobic membrane core from the aqueous surroundings on either side. This membrane inherently forms into a closed spherical vesicle to minimize free energy, thus self-assembling into a nanocapsule structure containing an aqueous lumen space protected and isolated from the surrounding aqueous environment by a thick (~10–20 nm) polymeric membrane.<sup>23</sup> We chose to encapsulate siRNA molecules within this aqueous lumen in this study, with the expectation that they would be effectively shielded from interaction with the external environment when encapsulated. The vast majority of nonviral gene delivery agents reported in the literature employ ionic complexation of negatively charged nucleotides to a positively charged delivery agent, and thus the encapsulation of siRNA within a vesicle represents an alternative modality for siRNA packaging and protection.<sup>17,24</sup> In addition, because of the thickness and hydrophobicity of a polymer vesicle membrane, permeability, and therefore leakage, is very low, even trending toward zero for charged molecules such as siRNA and

carboxyfluorescein.<sup>25</sup> Furthermore, polymer vesicle coronas, composed of a dense PEO brush layer, have been shown to effectively resist opsonization and therefore host immune response and clearance from the body.<sup>26,27</sup>

The polymer vesicles used in this study were further functionalized with peptide targeting ligands, to enhance cellular uptake and confer an active targeting modality to the vesicles, as shown schematically in Figure 1. Azide–alkyne “click” chemistry was utilized to covalently decorate the exterior surface of polymer vesicles with either the integrin binding GRGDSP peptide or an α<sub>5</sub>β<sub>1</sub> integrin binding peptide, named PR\_b (with amino acid sequence KSSPHSRN-(SG)<sub>5</sub>RGDSP).<sup>28–30</sup> The PR\_b peptide was designed to mimic the cell binding site of native fibronectin protein recognized by integrin α<sub>5</sub>β<sub>1</sub>.<sup>31</sup> It incorporates both the primary α<sub>5</sub>β<sub>1</sub> binding sequence, RGD, and the synergistic binding sequence, PHSRN, connected by an (SG)<sub>5</sub> linker, which was chosen to accurately mimic both the separation distance and the hydrophobicity/hydrophilicity of the linker region in the native fibronectin protein.<sup>32–34</sup> The design of PR\_b has been shown repeatedly to result in greatly improved adhesion and α<sub>5</sub>β<sub>1</sub> specificity over other RGD-containing peptide ligands.<sup>28,29,35–37</sup>

In this study, we investigated the ability of peptide-functionalized OB polymer vesicles to effectively deliver siRNA to breast cancer cells *in vitro*. Delivery to two different cell lines, MCF10A (immortalized but noncancer fibrocytic MCF10A breast cells) and T47D breast cancer cells, was investigated and compared. Both cell lines have been previously shown to express α<sub>5</sub>β<sub>1</sub> and adhere readily to fibronectin.<sup>38–41</sup> Both GRGDSP and PR\_b peptide-functionalized polymer vesicles were evaluated for effective delivery to these cell lines, and binding specificity to cell surface integrins was examined for PR\_b-functionalized vesicles using blocking peptides. Delivery of PR\_b-functionalized polymer vesicles to these cells was visualized by fluorescent confocal microscopy, and colocalization with cellular endosomes and lysosomes was assessed by organelle staining. Finally, the ability of PR\_b-functionalized polymer vesicles to effectively encapsulate and deliver siRNA to breast cancer cells was studied, and the effect of siRNA delivery on cell viability for both the cancerous T47D cells and the MCF10A cells was assessed. siRNA delivery by

polymer vesicles was also compared to that by a commercial siRNA transfection agent.

## MATERIALS AND METHODS

**Materials.** Unless otherwise noted, all chemicals were obtained from Sigma-Aldrich (St. Louis, MO) and used as received. Peptides PR\_b and GRGDSP were custom synthesized and obtained on the bead, with the side groups protected, from the Microchemical Facility at the University of Minnesota. The extruder and the 200 nm extrusion membranes were obtained from Avestin Inc. (Ottawa, Canada). The MCF10A and T47D epithelial human breast cells were obtained from ATCC (Manassas, VA). Cellular stains used in confocal imaging, the RiboGreen assay kit, and cell culture media and supplements were obtained from Invitrogen (Carlsbad, CA). Fetal bovine serum (FBS) was obtained from Atlas Biologicals (Fort Collins, CO). Human fibronectin-coated round coverslips were purchased from BD Biosciences (San Jose, CA). Small interfering RNA, siOrai3 (siGENOME siRNA Orai3, catalog number D-015896-04, antisense sequence 5'-CCAGUUCAAAACACGGGU-3'), and siControl (siGENOME Non-Targeting siRNA #2, catalog number D-001210-02, antisense sequence 5'-UAAGGCUAUGAAGAGAUAC-3') were obtained from Dharmacon Inc. (Chicago, IL).

**Polymer Synthesis.** Poly(ethylene oxide)-*b*-poly(1,2-butadiene) (OB) was synthesized sequentially using previously published anionic polymerization techniques.<sup>42</sup> First, hydroxyl-terminated poly(1,2-butadiene) (PB) homopolymer was synthesized. Next, in a separate reaction, the poly(ethylene oxide) (PEO) block was grown off the end of the PB block to form the OB diblock.

**Synthesis of Azide-Terminated OB (OB-N<sub>3</sub>).** The hydroxyl end group of the OB polymer was replaced with an azide group via mesylation followed by reaction with sodium azide. The details of this synthesis have been previously reported.<sup>28</sup>

**Synthesis of Alkyne-Terminated Peptides.** A terminal alkyne functional group was attached to the PR\_b and GRGDSP peptides to enable the “click” conjugation of these peptides with OB-N<sub>3</sub>. The details of this synthesis have been previously reported.<sup>28</sup>

**Polymer Vesicle Formation.** Polymer vesicles were prepared by self-assembly of the OB diblock in aqueous solutions using film rehydration.<sup>43</sup> OB and OB-N<sub>3</sub> polymers were placed in a vial in the desired ratio, and chloroform was added to form a concentrated polymer solution (~100 mg/mL). The mixture was gently shaken at room temperature for 24 h. Films were formed by drying, with all traces of chloroform removed using a high vacuum. An aqueous solution was then added to the film to form a 1% (w/w) (or 5% for siRNA encapsulation) solution of polymer. For the samples encapsulating carboxyfluorescein (CbF), either 3.0 or 80.0 mM CbF in phosphate buffered saline (PBS) was added, and for samples encapsulating siRNA, a solution of 6 μM siRNA and 5 μM RNAsure (Ambion, Grand Island, NY) was added. To remove any traces of RNase, samples incorporating siRNA were heated while stirring to 60 °C for the first 15 min (when heated, the RNAsure becomes active and neutralizes any RNase present) after adding the aqueous solution to the polymer film, and then stirred at 45 °C for 2 days before being allowed to cool to room temperature. After a few days of being stirred, polymer vesicles were fully dispersed. Vesicles were extruded at 60 °C through polycarbonate membranes with well-defined 200 nm pore sizes. After extrusion, each vesicle sample was characterized by dynamic light scattering (DLS) using a 90 Plus BI-MAS instrument (Brookhaven Instrument Co.) to determine the size distribution.

**Peptide Conjugation.** The PR\_b and GRGDSP peptides were conjugated onto the surface of the preformed polymer vesicles using the azide–alkyne “click” Huisgen cycloaddition reaction.<sup>44</sup> To a dispersion of vesicles at 4 °C was added a 2-fold excess of alkyne terminated peptide and copper sulfate (1.1 mM), sodium ascorbate (5.5 mM), and bathophenanthrolinedisulfonic acid (2.2 mM).<sup>45–47</sup> The reaction was allowed to come to room temperature and stirred for 24 h, after which a 5-fold excess, with respect to copper, of EDTA (ethylenediaminetetraacetic acid) was added to the solution to sequester the copper. The vesicle samples were then purified by

dialysis in PBS with Spectra/Por 6 dialysis tubing (50 kDa MWCO, Spectrum Laboratories, Rancho Dominguez, CA). The samples were dialyzed for a total of 3 days with the dialysate being changed every 4–12 h for a total of six times. Samples used in colocalization studies were alternatively purified by passing through a Sepharose CL-4B gel filtration column, and then used in experiments immediately after purification. This was done primarily so that the vesicles encapsulating self-quenching concentrations of CbF could be more quickly purified.

**Peptide Quantification.** Quantification of the mol % of surface bound peptide on polymer vesicles was carried out as previously described, using a fluorescamine-based fluorescent assay.<sup>28</sup>

**Encapsulate Quantification.** The amount of either CbF or siRNA encapsulated in polymer vesicles was assessed as follows. For CbF quantification, a small volume of polymer vesicle sample was diluted into PBS + 10% Triton X-100 to give a final volume of 200 μL within a well of a black 96-well plate. Two concentrations of polymer vesicles were assayed for each formulation with six repeats of each: one expected to give approximately 0.01 μM CbF in the well and the other one-half of this. After samples were incubated for 1 h in the Triton solution at room temperature, fluorescence (485/528 ex/em) was measured on a SynergyMX fluorometer (BioTek, Winooski, VT). The fluorescence obtained from the vesicle samples was correlated with a standard curve constructed for free CbF dissolved in the identical buffer to enable calculation of the CbF concentration in the polymer vesicle sample.

The fluorescent Quant-iT RiboGreen RNA Assay Kit (Invitrogen, Grand Island, NY) was used to quantify the amount of siRNA encapsulated within polymer vesicles. First, a standard curve was constructed for both the siOrai3 and the siControl siRNAs as per the manufacturer’s published protocol, with the concentration of siRNA in each stock solution measured on a NanoDrop 2000c spectrophotometer (Thermo Scientific, Waltham, MA). For the analysis of the siRNA content of vesicle samples, the polymer was first extracted out of solution, and then the liberated siRNA was quantified with the RiboGreen reagent. To 140 μL of RNase-free Tris-EDTA (TE) buffer was added 10 μL of polymer vesicle sample in an RNase-free microtube. Next, 1 mL of HPLC grade chloroform was added to the microtube, and the mixture was shaken vigorously. The microtube was centrifuged at 16 000g for 5 min, and then 10 μL of the top aqueous phase containing the siRNA was added to 90 μL of TE buffer in a new microtube. To this was added 100 μL of a 200-fold dilution of RiboGreen reagent in TE buffer, and the total volume was mixed by pipetting up and down. The contents of the microtube were added directly into a well on a black 96-well plate, and fluorescence was measured (485/528 ex/em) on a SynergyMX fluorometer (BioTek, Winooski, VT) 3 min after adding the RiboGreen reagent. It should be noted that for each point on the standard curves an identical extraction procedure was carried out, and each measurement was performed in triplicate.

**Cell Culture.** T47D and MCF10A cells were grown in RGM (modified RPMI-1640 medium supplemented with 10% (v/v) FBS, 100 units/mL penicillin, 0.1 mg/mL streptomycin, 10 mM HEPES, and 10 μg/mL insulin) and DFGM (modified Dulbecco’s Modified Eagle Medium: Nutrient Mixture F-12, DMEM/F12, supplemented with 5% (v/v) FBS, 100 units/mL penicillin, 0.1 mg/mL streptomycin, 15 mM HEPES, 10 μg/mL insulin, 20 ng/mL epidermal growth factor, 0.5 μg/mL hydrocortisone, and 100 ng/mL cholera toxin), respectively, at 37 °C, 5% CO<sub>2</sub>. Growth media was replaced every 2 days, and cells were passaged when they reached ~70% confluence by treating with TrypLE Express (Invitrogen, Grand Island, NY), and reseeding in new flasks at lower cell densities. Only cells of passage number 1–5 were used in experiments.

**Cellular Delivery Quantification.** A fluorescence plate assay was used to quantify the binding and internalization of polymer vesicles to cells. To each well of a cell culture 24-well plate was added 0.5 × 10<sup>6</sup> cells in 150 μL of FBS restricted growth media (growth media with only 2% (v/v) FBS) without phenol red. Cells were allowed to adhere to the plate surface by incubating at 37 °C, 5% CO<sub>2</sub>. Up to 50 μL of polymer vesicle sample (diluted with PBS when necessary) with encapsulated CbF was added to each well to make the overall CbF

concentration in each well 1.0  $\mu\text{M}$ . Plates were incubated protected from light for 24 h at 37 °C, 5% CO<sub>2</sub>. Next, the plates were gently washed twice with PBS to remove any unbound polymer vesicles but leave the cells adhered to the plate. Plates were frozen at -80 °C to permeabilize the cells, and thawed at room temperature for 3 h. To completely break and dissociate the cells and the polymer vesicles, 500  $\mu\text{L}$  of Borate Buffer (100 mM borate, pH 8.6) with 5% (v/v) Triton X-100 was added to each well, and the plates were allowed to sit at room temperature for 3 h.<sup>48</sup> Finally, fluorescence was measured using a SynergyMX fluorometer (BioTek, Winooski, VT) at 485/516 (ex/em). Negative controls were also run where peptide conjugated polymer vesicles were delivered to wells containing no cells.

Blocking experiments were performed in a fashion identical to the protocol detailed above, with the following slight alterations. The blocked cells were preincubated with the integrin binding free peptide, GRGDSP, at 0.5 mg/mL for 1 h at 37 °C, 5% CO<sub>2</sub>. After this preincubation, polymer vesicle samples were added and incubated with the cells for 4 h at 37 °C, 5% CO<sub>2</sub>.

**Confocal Microscopy.** Cells were seeded onto fibronectin modified coverslips in FBS restricted growth media without phenol red and allowed to adhere. Polymer vesicle samples were added to the monolayer of cells to yield an overall CbF concentration of 1.0  $\mu\text{M}$  for all cases, except when polymer vesicles containing a self-quenching concentration of CbF were added, for which an overall CbF concentration of 5.0  $\mu\text{M}$  was used. For the organelle staining images, the CellLight Early Endosomes-RFP \*BacMam 2.0\* (Invitrogen, Grand Island, NY) early endosomal stain was added at this time at a concentration of 40 particles/cell as per the manufacturer's procedure. The cells were incubated with the vesicles at 37 °C, 5% CO<sub>2</sub> for 24 h. The Lysotracker Blue DND-22 was added directly to the media at the 22 h time point to give a final concentration of 100 nM. After the full 24 h incubation, the cells were prepared for confocal imaging by washing, fixing, staining, and mounting. The coverslips were gently washed twice with 37 °C fluorescence buffer (FB), PBS supplemented with 2.5% FBS. They were then incubated for 15 min at 37 °C in 4% (v/v) paraformaldehyde in PBS, to fix the cells. The coverslips were washed three times with 37 °C FB, followed by fluorescently staining the cells by incubating them with either a mixture of nuclear and cell membrane stains in FB for 10 min at 37 °C or a far-red cell membrane stain in FB for 10 min at room temperature. The cell membrane permeable blue fluorophore, Hoechst 33342 (2.0  $\mu\text{mol}/\text{mL}$ ), was used as a nuclear stain, and the cell impermeable red fluorophore, Alexa Fluor 594 wheat germ agglutinin (5.0  $\mu\text{g}/\text{mL}$ ), was used as a cell membrane stain for the confocal images in Figure 3. The far-red cell membrane stain Alexa Fluor 647 wheat germ agglutinin (5.0  $\mu\text{g}/\text{mL}$ ) was employed for the organelle stained confocal images in Figures 5–7. After the cells were stained, the coverslips were again washed three times with FB, and then mounted facedown onto glass cover slides with ProLong Gold antifade reagent (Invitrogen, Grand Island, NY). The slides were imaged immediately after preparation on an Olympus Fluoview 1000 confocal laser scanning microscope in the Biomedical Image Processing Laboratory at the University of Minnesota. Colocalization analysis was performed using the software ImageJ and the quantification procedure developed by Costes et al.<sup>49,50</sup>

**Cell Viability Assay.** The MTT cytotoxicity assay was used to test the effect of siRNA delivery on the viability of each cell line. Cells, either T47D or MCF10A, were seeded onto 96-well plates at 5000 or 2000 cells per well, respectively, in 150  $\mu\text{L}$  of the appropriate FBS restricted growth media without phenol red. Cells were allowed to adhere, and then 50  $\mu\text{L}$  of sample, polymer vesicles diluted in PBS, free siRNA in PBS, Lipofectamine RNAiMAX (Invitrogen, Grand Island, NY) complexed siRNA, or just PBS, was added to each well. For samples containing siRNA, a concentration of 50 nM was added to the wells, while for empty polymer vesicle samples, a concentration of polymer identical to the analogous siRNA containing vesicle sample was added. The delivery of siRNA to cells by Lipofectamine RNAiMAX (Invitrogen, Grand Island, NY) was carried out as per the manufacturer's published procedure. After the samples were added, the plates were incubated for 24 h at 37 °C, 5% CO<sub>2</sub>, and then 100  $\mu\text{L}$

of the supernatant media was carefully removed from each well, as to not disturb the adhered cells, and replaced with 100  $\mu\text{L}$  of full growth media without phenol red. After an additional 48 h of incubation at 37 °C, 5% CO<sub>2</sub>, 15  $\mu\text{L}$  of MTT reagent (4.75 mg/mL thiazolyl blue tetrazolium bromide in PBS) was added to each well, and the plates were incubated for 4 h more at 37 °C, 5% CO<sub>2</sub>. A solubilizing solution of 75% dimethyl sulfoxide (DMSO):25% H<sub>2</sub>O (v/v) plus 5% sodium dodecyl sulfate (SDS) (w/v) was added to the plates (150  $\mu\text{L}$  per well), and the plates were further incubated, protected from light, for 24 h at room temperature. Finally, the absorbance and background absorbance were measured at 570 and 690 nm, respectively, using a SpectraMax Plus spectrophotometer (Molecular Devices, Sunnyvale, CA).

**qRT-PCR Expression Quantification.** The level of Orai3 mRNA expression was assessed using quantitative real time reverse transcription polymerase chain reaction (qRT-PCR). First, an assay was designed and validated at the BioMedical Genomics Center (BMGC) at the University of Minnesota to reliably quantify Orai3 mRNA expression. The assay design was prepared using the Roche Universal Probe Library (UPL) technology. Each assay design generated a sequence for the forward primer, reverse primer, amplicon, and provided the UPL probe number (Orai3, forward 5'-CAGGCA-GAGTCAGATTCTG-3', reverse 5'-CAGACTGATGGG-GAAAATCC-3', UPL probe no. 24; ACTB, forward 5'-AAGTCCCTGCCsATCCTAAAA-3', reverse 5'-ATGCTAT-CACCTCCCTGTG-3', UPL probe no. 55; GAPDH, forward 5'-CTCTGCTCCTCCTGTTCGAC-3', reverse 5'-ACGAC-CAAATCCGTTGACTC-3', UPL probe no. 60). Each primer was ordered through the BMGC Oligonucleotide and Peptide Synthesis service using Integrated DNA Technologies (IDT, Coralville, IA).

To validate the primer probe sets, qPCR was carried out on a dilution series of complementary DNA (cDNA) using an ABI 7900 HT real-time PCR system (Applied Biosystems, Grand Island, NY) (2 min activation at 60 °C and 5 min denaturation at 95 °C, followed by 45 cycles of 10 s at 95 °C and 1 min at 60 °C). The primer probe set with the highest validated efficiency (97%) was selected for future use.

For expression quantification, cells were seeded at 1 million cells per well on a six-well plate in 1.4 mL of FBS restricted growth media. Cells were allowed to adhere, and then 100  $\mu\text{L}$  of sample was added to each well (diluted as needed in PBS). The samples added were identical to those used in the MTT cell viability studies (50 nM of siRNA, etc.). The plates were incubated for 24 h at 37 °C, 5% CO<sub>2</sub>, at which point 3 mL of full growth media was added to each well, and the plates were further incubated for another 24 h at 37 °C, 5% CO<sub>2</sub>. After the full 48 h of incubation, growth media was poured off the plate, and 1 mL of RNazol RT reagent (Molecular Research Center, Cincinnati, OH) was added immediately to each well. Total RNA from the cells in each well was isolated following the manufacturer's procedures. The final RNA isolate was dissolved in RNase-free water, and the concentration yielded was assessed with a NanoDrop 2000c spectrophotometer (Thermo Scientific, Waltham, MA). Then qRT-PCR was carried out using the RNA isolated from cells at BMGC to assess the mRNA expression levels for each sample of the gene of interest, Orai3, and two housekeeping genes, ACTB and GAPDH.

Total RNA samples were synthesized to first-strand cDNA using SuperScript II RT (Invitrogen, Grand Island, NY). Next, qPCR was carried out on these cDNA samples as previously detailed using an ABI 7900 HT. For each qPCR sample, 48 ng of cDNA was used along with forward primer, reverse primer, and probes each at a concentration of 10  $\mu\text{M}$ . Reverse transcriptase negative controls were run for each RNA isolation, and no DNA contamination of the total RNA isolate could be detected. The percentage knockdown of Orai3 was calculated relative to the geometric mean of the cycle thresholds,  $C_v$ , of both housekeeping genes (ACTB and GAPDH) using the  $\Delta\Delta C_t$  method.<sup>51,52</sup>

## RESULTS AND DISCUSSION

**Polymer Vesicle Formation.** Polymer vesicles were formed by simple film hydration of poly(1,2-butadiene)-*b*-

poly(ethylene oxide), PB-PEO or OB for short, block copolymer in aqueous solutions. The OB block copolymer was chosen because it has been extensively studied and shown to form a wide variety of self-assembled morphologies in aqueous solution, including vesicles, and because our previous work has shown that OB polymer vesicles could allow for some release of encapsulates after cellular internalization.<sup>53–57</sup> Thus, the OB polymer system represented a good model system with potential for biological efficacy. The full specifications for the OB block copolymers used to form vesicles in this study have been previously reported.<sup>28</sup> Briefly, OB block copolymers were synthesized by living anionic polymerization, to give polymers with narrow PDI (polydispersity index), 1.04, and number averaged molecular weight ( $M_n$ ) of 8.4 kDa. A weight percentage of PEO of 24% in the final block copolymer was targeted, because this weight percentage has previously been shown to form vesicles in solution for OB polymers of similar molecular weight.<sup>55</sup> Both PB and PEO are considered bioinert, and OB vesicles have shown promising early results both *in vitro* and *in vivo*.<sup>27,28,43</sup>

Vesicles encapsulating molecules of interest were formed by film hydration without the aid of any organic cosolvent, by simply introducing aqueous solutions of the molecule of interest to a dried film of OB polymer. After extrusion, the vesicle size was evaluated using dynamic light scattering (DLS) and was found to be  $249 \text{ nm} \pm 117 \text{ nm}$  (representative average hydrodynamic diameter for all vesicle samples used in this study). This vesicle size is on the high range of sizes able to take advantage of the enhanced permeability and retention effect; however, vesicles could easily be extruded down to much smaller sizes if needed for future applications.<sup>58</sup> For this *in vitro* study, the  $\sim 250 \text{ nm}$  size range was simply chosen and held to consistently. To functionalize these vesicles with peptide targeting ligands, azide–alkyne “click” conjugation chemistry was utilized. The details of this conjugation strategy have been previously reported in the literature.<sup>28,59,60</sup> For illustrative and comparative purposes, a single surface concentration of peptide ligand was used throughout this study, with an average mole percentage of peptide conjugation for all vesicle samples of  $21 \pm 1 \text{ mol \%}$  peptide. This degree of surface functionalization was chosen on the basis of our previous experience with peptide-functionalized polymer vesicles and their delivery to cancer cells, as it could be readily achieved using “click” chemistry surface conjugation, and it has elicited significant polymer vesicle internalization into cancer cells.<sup>28</sup> A strength of this “click” conjugation strategy is that every peptide ligand is conjugated to the exterior surface with identical orientation, specifically at the N-terminus of the peptide. Previous studies have demonstrated that ligand surface orientation can be critical for proper adhesion and interaction with cell surface adhesion molecules.<sup>61</sup>

For the experiments in this study, two encapsulates were used, siRNA and carboxyfluorescein (CbF). The use of CbF is advantageous for a number of reasons. It enables the encapsulation of high self-quenching concentrations of CbF (e.g., 80 mM) in polymer vesicles so that vesicle release can be visualized. This is perhaps the largest advantage of the use of CbF for this work, because whether OB polymer vesicles could release intracellularly and to what extent is an open question. Also, CbF is a highly anionic fluorescent dye molecule, which is membrane impermeable due to its negative charge, like siRNA, and is used as a vesicle encapsulate to allow effective experimental quantification and tracking of vesicles.<sup>56,62</sup> For

these reasons, CbF was elected to visualize encapsulate delivery and release rather than fluorescently labeled siRNA.

Two siRNA molecules were encapsulated: siOrai3, a siRNA specifically designed to target the Orai3 gene, and siControl, a nontargeting negative control siRNA designed to not target any gene present in the cells in this study. The average siRNA encapsulation efficiency across all of the vesicle samples tested was  $50.2 \pm 9.5\%$  with no discernible difference in the encapsulation efficiency between the two siRNA molecules, as might be expected given their similar molecular weights. This encapsulation efficiency is nearly twice that previously reported in the literature for alternate methods of encapsulation in polymersomes and liposomes.<sup>63,64</sup> The relatively high siRNA encapsulation efficiency indicates that very little siRNA degradation is observed. Moreover, after siRNA has been encapsulated within polymersomes, it remains protected from degradation, and within the limits of measurement no siRNA degradation was observed over weeks of vesicle storage at  $4^\circ\text{C}$  (encapsulated siRNA was quantified initially and after a couple weeks of storage, and no decrease in siRNA was observed).

**Delivery of Peptide-Functionalized Vesicles to MCF10A and T47D Cells.** Delivery of peptide-functionalized polymer vesicles to two different cell lines, MCF10A and T47D, was investigated in this study. MCF10A is a human cell line that originated from spontaneous immortalization of breast epithelial cells obtained from a patient with fibrocystic disease, and is frequently used as a model cell line for noncancerous human breast cells.<sup>65</sup> T47D cells are human epithelial cancerous breast cells that have been previously shown to highly overexpress Orai3 over both normal human mammary epithelial cells obtained directly from patients and MCF10A cells.<sup>6</sup> These two cell lines allowed us to contrast delivery of siRNA to cancerous breast cells, T47D, and noncancerous MCF10A cells.

Previous reports by our group have found peptide-functionalized vesicles (both polymersomes and liposomes), especially PR\_b-functionalized vesicles, to effectively deliver to a variety of cancer cell lines; however, delivery to the MCF10A and T47D cell lines remained untested.<sup>28,35–37,66</sup> CbF encapsulated fluorescent polymer vesicles were utilized to investigate delivery of peptide-functionalized vesicles to the cancerous T47D breast cell line and the MCF10A breast cell line. Polymer vesicles encapsulating the fluorescent dye, CbF, were functionalized with either the simple GRGDSP peptide or the PR\_b peptide. These vesicles were introduced, at a total overall concentration of  $1 \mu\text{M}$  CbF, to the media surrounding growing monolayers of cells, and then allowed to incubate with the cells at  $37^\circ\text{C}$  for 24 h. After that, the cell monolayer was extensively washed to remove any vesicles that were not bound to or internalized within cells, and subsequently either lysed and the total CbF delivered quantified (Figure 2) or were imaged by confocal microscopy (Figure 3).

Figure 2 shows quantification of the level of binding and internalization (termed delivery when considered together) of peptide-functionalized vesicles to the two contrasted cell lines. Very minimal delivery of nonfunctionalized vesicles, the 0% peptide case, is observed for both cell lines. This is as expected, considering the fully PEGylated surface of these nonfunctionalized vesicles is known to resist nonspecific adhesion and protein interactions.<sup>26</sup> Akin to “stealth” liposomes, the PEG chains coating the surface of the vesicles create a steric barrier to adhesion, and therefore active internalization by the cells.<sup>43,67</sup> The limited amount of delivery that is observed for

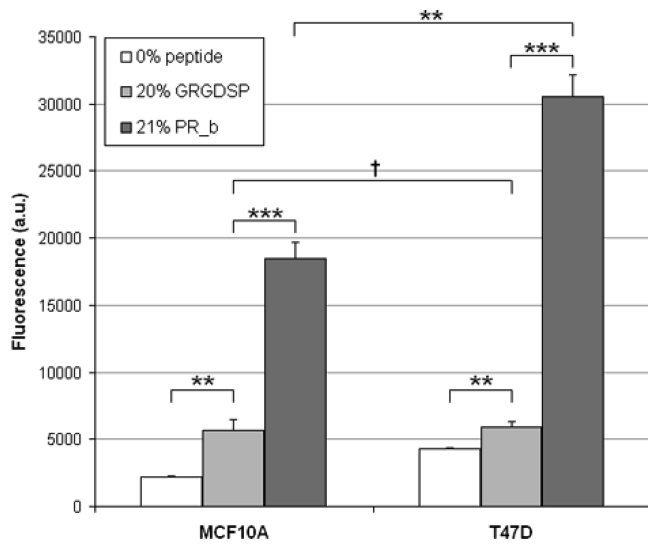


**Figure 2.** Delivery of the CbF fluorophore encapsulated within peptide-functionalized polymer vesicles to either MCF10A breast cells or T47D cancerous breast cells. Cells were incubated with CbF loaded polymer vesicles functionalized with the mol % of peptide noted in the figure for 24 h at 37 °C, after which the amount of delivery for each case was quantified. Data are the mean  $\pm$  standard error of three separate experiments ( $n = 3$ ), with each experiment performed in triplicate. Students *t* test statistical analyses were performed, and the statistical significances were noted for the bracketed data ( ${}^{\dagger}p > 0.05$  indicating no statistically significant difference,  $*p < 0.05$ ,  $**p < 0.01$ ,  $***p < 0.001$ ).

the nonfunctionalized vesicles is likely due to nonspecific pinocytosis of the surrounding media by the cells.<sup>63,68</sup> Polymer vesicles functionalized with the targeting peptides, GRGDSP and PR<sub>b</sub>, are thought to internalize by a more active route involving cell surface integrin binding followed by active cellular internalization.<sup>28,35</sup> Vesicles functionalized with the peptide ligand, GRGDSP, performed better than nonfunctionalized vesicles for both cell lines. However, the increase in delivery observed for GRGDSP-functionalized vesicles is minimal in comparison to PR<sub>b</sub>-functionalized vesicles, and additionally no statistically significant difference in delivery was seen for GRGDSP-functionalized vesicles between the two cell lines. In contrast, polymer vesicles functionalized with the PR<sub>b</sub> peptide delivered much more effectively to both cell lines than either nonfunctionalized vesicles or GRGDSP-functionalized vesicles, giving 7 times the delivery of nonfunctionalized vesicles and 5 times the delivery of GRGDSP-functionalized vesicles for T47D cells. The PR<sub>b</sub>-functionalized vesicles yielded significantly greater levels of delivery in the cancerous T47D cells as compared to the noncancerous MCF10A cells, a distinction that GRGDSP-functionalized vesicles were not able to achieve. It is unclear at this time what causes PR<sub>b</sub>-functionalized polymer vesicles to deliver more effectively to T47D cells as opposed to MCF10A cells. However, one likely explanation lies in the relative expression level of  $\alpha_5\beta_1$  integrin on the surface of each cell line, as there is evidence in the literature that T47D cells may have more  $\alpha_5\beta_1$  integrin surface expression than MCF10A cells.<sup>38,69</sup>

Confocal microscopy of polymer vesicles delivered to cells (Figure 3) was performed to corroborate the results shown in

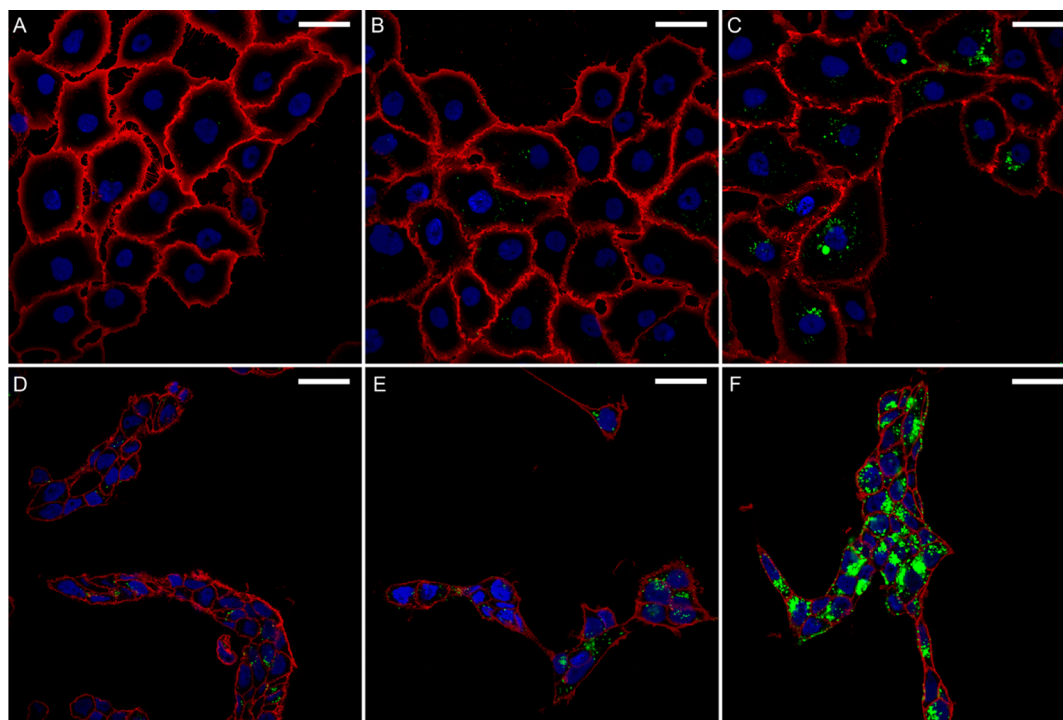


**Figure 3.** Confocal microscopy images of polymer vesicle delivery to MCF10A breast cells (A–C) and breast cancer T47D (D–F) cells. Cells were incubated with CbF loaded polymer vesicles functionalized with 0 mol % peptide (A,D), 20 mol % GRGDSP (B,E), and 21 mol % PR<sub>b</sub> peptide (C,F) for 24 h at 37 °C, after which cells were fixed, stained, and imaged. Polymer vesicles encapsulating 3 mM of CbF were delivered to cells at a concentration of 1  $\mu$ M CbF. Nuclei are stained blue, cell membranes red, and polymer vesicles encapsulating CbF are shown as green. Internalization of polymer vesicles is shown by the presence of green within the confines of the red cell membranes. All scale bars are 30  $\mu$ m. The images show a slice from the interior of the cells, at a “z-height” approximately 2  $\mu$ m above the bottom coverslip surface to which cells are adhered.

Figure 2 and to gain a better understanding of polymer vesicle delivery. Fluorescent polymer vesicles were delivered to cells identically to the procedure used to quantify delivery (Figure 2), only after the 24 h incubation period cells were fixed and stained for imaging rather than being lysed for fluorescence quantification. For the images shown in Figure 3, the cell plasma membranes were stained red, the cell nuclei were stained blue, and CbF, the fluorescent encapsulate delivered by the polymer vesicles, appears green. Each cell monolayer was imaged  $\sim 2 \mu\text{m}$  above the surface of coverslip on which they were grown, so that the confocal images shown are a slice from within the cell. Thus, in these images, simple surface binding can be differentiated from actual internalization within the cell. Whenever the green of the CbF fluorophore appears within the confines of a red cell wall, this indicates internalization of the polymer vesicles, and it is clear in all of the images in Figure 3 that the vast majority of delivery is by internalized vesicles and not simply surface bound vesicles. As in Figure 2, either nonfunctionalized, GRGDSP-functionalized, or PR\_b-functionalized polymer vesicles were delivered to both cell lines, MCF10A and T47D. Although it is always dubious to extrapolate the delivery observed in the relatively small sample population contained within a confocal image to more quantitative measures of delivery, the levels of delivery observed in Figure 3 do agree, at least on a qualitative basis, with the levels of delivery measured in Figure 2. The nonfunctionalized polymer vesicles (0% peptide) give very minimal delivery; green dots are very occasionally observed within a cell. Also, slightly higher delivery of nonfunctionalized vesicles is observed for T47D cells as compared to MCF10A cells. Slightly more delivery is observed for GRGDSP (20 mol % GRGDSP)-functionalized vesicles for both cell lines. However, dramatically more internalization is seen for PR\_b (21 mol % PR\_b)-functionalized vesicles, especially for T47D cells. A common feature of all of the confocal images presented in Figure 3 is that the green CbF vesicle encapsulate is for a large part localized within punctate dots within the cells. These green fluorescing bodies within the cells are clearly much larger than the size of the polymer vesicles ( $\sim 250 \text{ nm}$ ), so it is inferred that these bodies are in fact intracellular organelles (likely endosomes and lysosomes). It is difficult to determine from Figure 3 whether the encapsulate is effectively released from the polymer vesicles or moreover whether the encapsulate can escape the intracellular organelles that they are likely contained within, but these questions will be dealt with later in this Article.

Taken together, the results of Figures 2 and 3 clearly demonstrated that PR\_b-functionalized vesicles were highly effective at delivering to both cell lines, but especially the cancerous T47D cells. Moreover, PR\_b-functionalized vesicles were delivered at levels many times greater than those observed for GRGDSP-functionalized vesicles and exhibited enhanced delivery to cancerous T47D cells not seen for GRGDSP-functionalized vesicles. Considering these results, the decision was made to focus the rest of our investigations solely on PR\_b-functionalized vesicles, as they were clearly delivering much more effectively, and were thus the best prospect for successful siRNA delivery.

To better characterize the nature of binding and internalization for PR\_b-functionalized vesicles, integrin blocking studies were conducted (Figure 4). Cell surface integrins were blocked by adding a high concentration of free (i.e., not conjugated to a polymer chain) GRGDSP peptide to the media

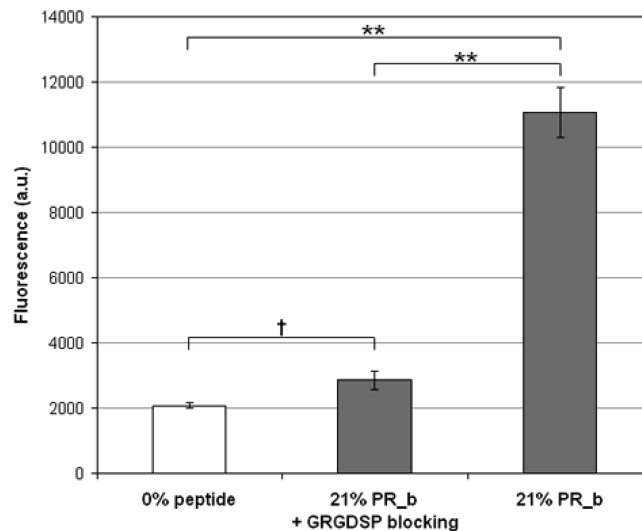


**Figure 4.** Delivery of CbF encapsulated within PR\_b-functionalized polymer vesicles to either unblocked T47D cells or T47D cells with their surface integrins blocked by GRGDSP peptides free in solution. Cells were incubated with CbF loaded polymer vesicles functionalized with 21 mol % PR\_b for 4 h at 37 °C, after which the amount of delivery for each case was quantified. Data are the mean  $\pm$  standard error of three separate experiments ( $n = 3$ ), with each experiment performed in triplicate. Students *t* test statistical analyses were performed, and the statistical significances were noted for the bracketed data ( $\dagger p > 0.05$ ,  $*p < 0.05$ ,  $**p < 0.01$ ,  $***p < 0.001$ ).

that the cell monolayers were growing in. Next, PR\_b-functionalized polymer vesicles were added to the cell media and allowed to deliver over the course of a 4 h incubation period at 37 °C. Delivery was then quantified in a fashion identical to that employed in the quantification experiments shown in Figure 2. Figure 4 compares the level of delivery for PR\_b-functionalized polymer vesicles to integrin blocked T47D cells, to the levels of unblocked delivery for both nonfunctionalized vesicles and PR\_b-functionalized vesicles. All of the data shown in Figure 4 are for the same 4 h incubation, and this shorter incubation time is the reason for the lower fluorescence values shown in Figure 4 as compared to those in Figure 2. For the unblocked case, PR\_b-functionalized vesicles are again shown to give higher levels of delivery than nonfunctionalized vesicles, as would be expected. However, when cell surface integrin binding sites are blocked by GRGDSP peptides, the level of delivery for PR\_b-functionalized vesicles drops to approximately that observed for nonfunctionalized vesicles. Short RGD containing peptides, such as GRGDSP, have been shown to bind to a wide variety of cell surface integrins, so they are a convenient molecule to use for blocking integrin adhesion.<sup>70</sup> Next, because delivery of PR\_b-functionalized vesicles is nearly completely reduced to the levels seen for nonfunctionalized vesicles by GRGDSP blocking, it can be inferred that PR\_b-functionalized vesicles are primarily internalized by specific adhesion to cell surface integrins followed by uptake, and not by nonspecific adhesion or nonspecific uptake routes. This result is corroborated by previous results from our group, including results demonstrating that delivery of PR\_b-functionalized polymer vesicles is mitigated by  $\alpha/\beta_1$ -receptor mediated endocytosis as demonstrated by blocking experiments with anti- $\alpha/\beta_1$  antibody and by delivering to cell lines with different levels of  $\alpha/\beta_1$  expression.<sup>28</sup>

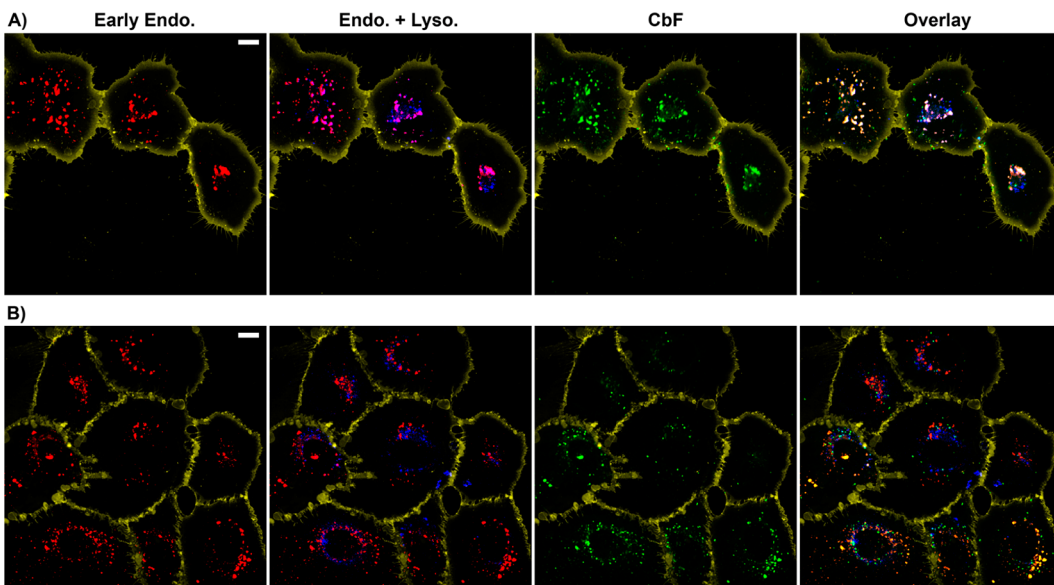


**Figure 5.** Confocal microscopy images showing colocalization of CbF delivered by PR<sub>b</sub>-functionalized polymer vesicles with stained endosomes and lysosomes in MCF10A cells. Cells were incubated with PR<sub>b</sub>-functionalized polymer vesicles for 24 h at 37 °C, after which cells were imaged. (A) 20 mol % PR<sub>b</sub>-functionalized polymer vesicles encapsulating 3 mM CbF, delivered to cells at a concentration of 1 μM CbF. (B) 21 mol % PR<sub>b</sub>-functionalized polymer vesicles encapsulating 80 mM CbF, a self-quenching concentration, delivered to cells at a concentration of 5 μM CbF. Cell membranes were stained yellow, early endosomes were stained red, all acidic organelles (endosomes and lysosomes) were stained blue, and polymer vesicle delivered CbF appears green. All scale bars are 10 μm. The images show a slice from the interior of the cells, at a “z-height” approximately 2 μm above the bottom coverslip surface to which cells are adhered.

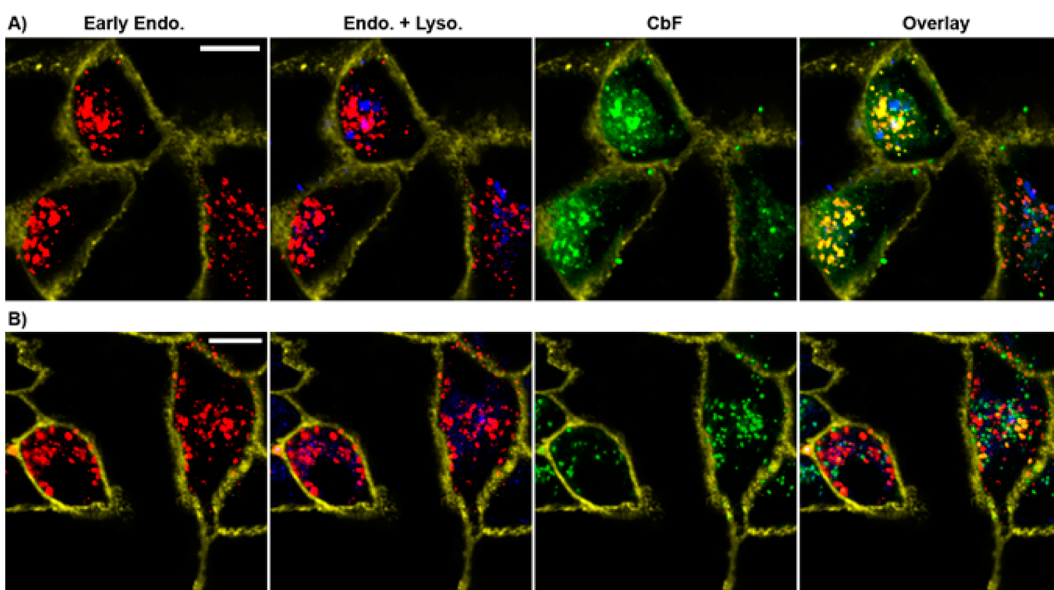


**Figure 6.** Confocal microscopy images showing colocalization of CbF delivered by PR<sub>b</sub>-functionalized polymer vesicles with stained endosomes and lysosomes in T47D cells. Cells were incubated with PR<sub>b</sub>-functionalized polymer vesicles for 24 h at 37 °C, after which cells were imaged. (A) 20 mol % PR<sub>b</sub>-functionalized polymer vesicles encapsulating 3 mM CbF, delivered to cells at a concentration of 1 μM CbF. (B) 21 mol % PR<sub>b</sub>-functionalized polymer vesicles encapsulating 80 mM CbF, a self-quenching concentration, delivered to cells at a concentration of 5 μM CbF. Cell membranes were stained yellow, early endosomes were stained red, all acidic organelles (endosomes and lysosomes) were stained blue, and polymer vesicle delivered CbF appears green. All scale bars are 10 μm. The images show a slice from the interior of the cells, at a “z-height” approximately 2 μm above the bottom coverslip surface to which cells are adhered.

This body of evidence along with the results of Figure 4 suggest that delivery may be  $\alpha_5\beta_1$ -mediated.

**Visualization of Intracellular Encapsulate Release with Organelle Colocalization.** To better understand the intracellular fate of polymer vesicles and any encapsulates they hold, fluorescence colocalization studies were performed. Prior to these studies, relatively little was known about the pathway

of internalization of PR<sub>b</sub>-functionalized polymer vesicles and the degree of intracellular release upon internalization within cells.

PR<sub>b</sub>-functionalized polymer vesicles encapsulating CbF were introduced to MCF10A (Figure 5) and T47D (Figures 6 and 7) cells, and after a 24 h incubation at 37 °C any polymer vesicles that were not delivered were washed away and the cells

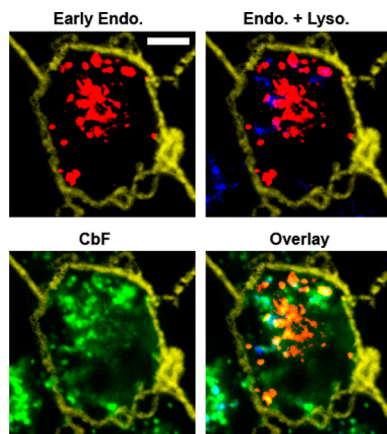


**Figure 7.** Confocal microscopy images showing colocalization of CbF delivered by PR<sub>b</sub>-functionalized polymer vesicles with stained endosomes and lysosomes in T47D cells. Cells were incubated with 20 mol % PR<sub>b</sub>-functionalized polymer vesicles for 24 h at 37 °C, after which cells were imaged. The polymer vesicles were encapsulating 3 mM CbF and were delivered to cells at a concentration of 1 μM CbF. Cells membranes were stained yellow, early endosomes were stained red, all acidic organelles (endosomes and lysosomes) were stained blue, and polymer vesicle delivered CbF appears green. The scale bar is 5 μm. The images show a slice from the interior of the cells, at a “z-height” approximately 2 μm above the bottom coverslip surface to which cells are adhered.

were imaged by confocal microscopy. Intracellular organelles were fluorescently stained, so that fluorescence from the CbF vesicle encapsulate (shown as green in Figures 5–7) could be colocalized with the organelles of interest. On the basis of the punctate nature of the CbF fluorescence shown in Figure 3, we speculated that polymer vesicles were likely primarily contained within intracellular organelles, and the most likely candidates for those organelles would be endosomes and lysosomes. Thus, we stained these organelles for colocalization. Early endosomes were stained with the CellLight Early Endosomes-RFP transfection-based fluorescent tag (shown as red in Figures 5–7). This fluorescent tag is highly specific for early endosomal organelles as it operates by transfecting the cell with the red fluorescent protein (RFP) tagged to the Rab5a protein, an early endosomal marker. For late endosomal and lysosomal staining, the Lysotracker Blue stain was utilized (shown as blue in Figures 5–7). This stain consists of a weakly basic fluorophore that preferentially accumulates in acidic intracellular compartments and is thus staining all acidic compartments within the cell including both lysosomes and endosomes (early and late). This can be clearly seen by colocalization of blue with red in Figures 5–7. Thus, in these figures, early endosomes are stained red, lysosomes, early, and late endosomes are all stained blue, and the polymer vesicles encapsulating CbF fluoresce green. In addition, a far-red cell membrane stain has been applied to the cells to clarify the boundaries of each cell, and this is shown as yellow in the images.

Two different PR<sub>b</sub>-functionalized polymer vesicle formulations were delivered to each cell line: one containing 3 mM CbF delivered at 1 μM within 20 mol % PR<sub>b</sub>-functionalized polymer vesicles (Figures 5A and 6A), and the other containing a self-quenching concentration of CbF (80 mM), delivered at 5 μM (so that CbF fluorescence could be seen clearly), within 21 mol % PR<sub>b</sub>-functionalized vesicles (Figures 5B and 6B).

While the vesicles with the 3 mM CbF concentration allow us to visualize the encapsulate within the cell, the self-quenching vesicles allow us to clearly visualize encapsulate release. For the vesicles with the 80 mM CbF concentration, the CbF is at a high enough concentration that it is effectively self-quenching and therefore nonfluorescent, so that only after the encapsulate has been released and diluted does it appear in the confocal images. Therefore, delivery of polymer vesicles containing self-quenching concentrations of CbF allows us to address the question of whether an encapsulate that is charged as the CbF (and siRNA) delivered by PR<sub>b</sub>-functionalized OB polymer vesicles can be effectively released.

Confocal images showing organelle colocalization for the delivery of PR<sub>b</sub>-functionalized polymer vesicles are presented in Figure 5 for MCF10A cells and Figure 6 for T47D cells. Delivery of polymer vesicles containing a lower concentration of CbF is shown on top (Figures 5A and 6A), and delivery of polymer vesicles containing a self-quenching concentration of encapsulate is shown on the bottom (Figures 5B and 6B). First, from Figures 5A and 6A it is clear that for both cell lines the polymer vesicle encapsulate is highly colocalized with the early endosomes, as well as, to some degree, the late endosomal and lysosomal compartments. Looking at the self-quenching series of images (Figures 5B and 6B), where encapsulate release is selectively visualized, it can be seen that the vesicle encapsulate is being released in the early endosomes as well as the late endosomes and lysosomes, with more release apparent in the early endosomes. It is interesting that we observe release from these not explicitly degradable OB polymer vesicles, and the mechanism of this release is currently not fully understood. It is well established that the enzymatic low pH slurry that exists within cellular lysosomes is significantly more degradative than a simple acidic solution.<sup>71</sup> Additionally, one potential hypothesis is that the double bonds in the polybutadiene block of the OB polymer could be oxidized within the cell, thus leading to a reduction in hydrophobicity and polymer vesicle destabilization; however, this hypothesis needs detailed investigation.

A general feature of these images is that, although the polymer vesicle encapsulate colocalizes well with the endosomes and lysosomes, there is also a distinct amount of hazy, diffuse green surrounding many of the more punctate spots of fluorescence. This feature is most distinct in the T47D cell images (Figures 6 and 7). Figure 7 shows a blown up image of a single T47D cell, that is not shown in Figure 6, which clearly shows this diffuse encapsulate fluorescence. In these images, background fluorescence was rigorously subtracted, and we are quite confident that the diffuse green fluorescence seen in these images is not autofluorescence of the cells, but we hypothesize that it may be visualization of CbF escape from the organelles into the cytosol. Extra-cellular release of CbF from these nonleaky, thick walled polymer vesicles followed by leakage into the cells is not a concern as evidenced by the lack of hazy fluorescence in Figure 3A and D, so that any CbF visualized in Figures 6 and 7 likely derives from intracellular activated release. This escape from the organelles and into the cytosol is highly relevant for delivery of siRNA, because siRNA must be able to escape the endosome or lysosome and reach the cytosol of the cell for it to be effective. This ability of polymer vesicles to facilitate some escape of encapsulates from endosomes and lysosomes could be instrumental to successful delivery of siRNA. Previous studies for biodegradable polymer vesicles have demonstrated that escape from acidic organelles can be

facilitated by polymer vesicles through a route thought to involve pore formation in the walls of the endosomes and lysosomes.<sup>20,63,68</sup> However, it is dubious whether a similar mechanism could be at play with the OB polymer vesicles studied here, as the membrane lytic properties observed were thought to derive from partially degraded block copolymer chains behaving similar to small molecule surfactants.

The levels of colocalization of the polymer vesicle encapsulate delivered with the early endosomes and with both the endosomes and the lysosomes were quantified for the images shown in Figures 5 and 6. The percentage of the total green fluorescence intensity that colocalizes with the intracellular organelles of interest is tabulated for each case in Table 1. From the colocalization values reported in Table 1, a

**Table 1. Colocalization Quantification of Delivered Fluorophore with Intracellular Organelles**

cells	colocalization with early endo. <sup>a</sup>	colocalization with endo. + lyso. <sup>b</sup>
Polymersomes Encapsulating 3 mM CbF <sup>c</sup>		
MCF10A	58%	67%
T47D	56%	62%
Polymersomes Encapsulating 80 mM CbF <sup>d</sup>		
MCF10A	57%	61%
T47D	47%	54%

<sup>a</sup>Colocalization of carboxyfluorescein (CbF) with stained early endosomes, reported as the percentage of overall CbF intensity that colocalizes. <sup>b</sup>Colocalization of CbF with all acidic organelles (endosomes and lysosomes), reported as the percentage of overall CbF intensity that colocalizes. <sup>c</sup>Colocalization quantified for images shown in Figures 5A and 6A, where polymer vesicles encapsulating 3 mM carboxyfluorescein (CbF) were delivered to cells. <sup>d</sup>Colocalization quantified for images shown in Figures 5B and 6B, where polymer vesicles encapsulating 80 mM carboxyfluorescein (CbF), a self-quenching concentration, were delivered to cells.

couple of points hold true for the cases tested. First, although the CbF encapsulate colocalizes with both endosomes and lysosomes, a large majority of the encapsulate localized within the early endosomes. This is likely an important point for the effective delivery of siRNA, as the environment within early endosomal compartments is milder, and therefore less likely to rapidly degrade any released siRNA, as opposed to the harsh environment within a lysosome. Along these lines, for the self-quenching polymer vesicles (Figures 5B and 6B), it is clear that a majority of the colocalized encapsulate is not only localized within the early endosomes, but is in fact released within the early endosomes. Second, the amount of CbF that is released in the cellular organelles is similar to the amount that is localized in the endosomes and lysosomes after 24 h. Considering that these experiments were performed after 24 h, it may not be too surprising that there is not that big of a difference between the results from the 3 and 80 mM CbF concentrations. The utility of the 80 mM self-quenching experiments is not lost, however, in that they demonstrated that OB polymer vesicles are capable of intracellular release of encapsulates (a previously unanswered question). Third, there is a notable percentage of encapsulate that is not accounted for in the percentages and is therefore not colocalized with either the endosomes or the lysosomes. This may likely be the diffuse green that is seen in the cytosol of the images in Figures 5–7, and we hypothesize that it may represent some escape of encapsulate from the cellular organelles into the cell cytosol. As discussed previously,

achieving endosomal and lysosomal escape is critical to attaining effective siRNA delivery.

**siRNA Delivery by PR\_b-Functionalized Vesicles to T47D and MCF10A Cells.** To the knowledge of the authors, only a few previous studies have dealt with delivery of siRNA by polymer vesicles, and these works investigated significantly different systems, in terms of siRNA, cells, and polymer.<sup>63,72</sup> Furthermore, these previous reports dealt with nontargeted delivery; thus the effect of functionalizing the polymer vesicles with a targeting ligand, such as the PR\_b peptide, was not studied. We sought to investigate the proficiency with which PR\_b-functionalized polymer vesicles could be utilized to deliver a novel siRNA therapeutic, siOrai3, to the breast cancer cell line, T47D. Additionally, the effect of siOrai3 delivery to cancerous T47D cells was contrasted to the effect of delivery to noncancerous MCF10A cells.

Although it is clear from the results presented thus far that PR\_b-functionalized OB polymer vesicles themselves deliver with high efficacy to both T47D and MCF10A cells, effective delivery of siRNA is a further level of complexity. The siRNA must first be protected from degradation before it is internalized within the cell, and then it must be effectively released from the polymer vesicles and make its way to the cytosol, where it can assemble with the endogenous RISC protein complex to effect the desired mRNA knockdown. As discussed previously, two siRNA molecules, siOrai3 and siControl, were encapsulated inside of polymer vesicles, and their effect on cells was compared. siOrai3 is a siRNA that specifically targets the Orai3 gene for RNAi knockdown. It has previously been shown in the literature that knockdown of Orai3 expression can specifically arrest cell cycle progression for T47D breast cancer cells, eventually leading to apoptosis and a reduction in cell viability, but has a minimal effect on the cell viability of noncancerous breast cells.<sup>6</sup> So it was expected that siOrai3 could behave as a cancer cell-specific therapeutic in our experiments. The siControl sequence chosen in this study targets firefly luciferase mRNA and therefore is used as a nontargeting siRNA as it does not target any of the genes present in either T47D cells or MCF10A cells. Thus, siControl gives a baseline cellular siRNA response for comparison with that of siOrai3.

The two siRNA molecules, siOrai3 and siControl, were delivered to MCF10A and T47D cells in a variety of forms, and the resultant effects on cell viability and Orai3 knockdown were measured (Figures 8 and 9). Figure 8 shows the effect of siOrai3 delivery for each of the varying formulations on cell viabilities and Orai3 knockdown normalized to the appropriate siControl case, and Figure 9 shows all of the control cases (delivery of siControl and delivery of “empty” polymer vesicles) with values normalized to untreated cells. Delivery of siOrai3 encapsulated within polymer vesicles was compared to delivery of free siOrai3 in solution, and to siOrai3 complexed with a commercial transfection agent, Lipofectamine RNAi-MAX. A consistent siRNA delivery concentration of 50 nM was used for all siRNA formulations. Cell viability was assessed at 72 h using the MTT assay, and Orai3 mRNA expression levels were assessed at 48 h using qRT-PCR.

As seen in Figure 8, siOrai3 either as free siRNA in solution (siOrai3) or encapsulated in nonfunctionalized polymer vesicles (0% PR\_b siOrai3) gave no statistically significant change in cell viability or Orai3 expression for either cell line with respect to cells treated with siControl. Without the aid of some delivery agent, free siRNA has very little chance of

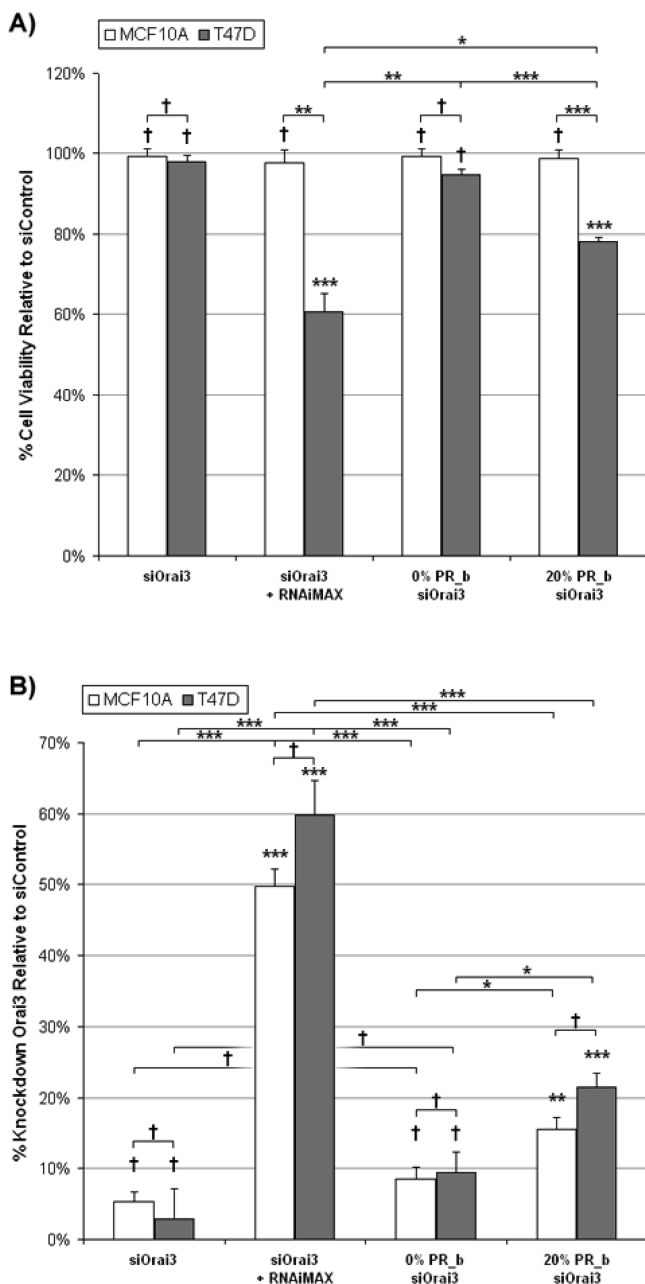


**Figure 8.** Percent cell viabilities (A) and knockdown of Orai3 (B) in MCF10A breast cells and T47D breast cancer cells after treatment with the indicated siOrai3 formulations. Cells were incubated with 50 nM of siOrai3 delivered as a formulation with the indicated delivery agents for 24 h at 37 °C, after which the cell medium was refreshed and incubation continued. (A) Cell viability was quantified using the MTT assay at 72 h after siOrai3 delivery. Data are the mean  $\pm$  standard error of three separate experiments ( $n = 3$ ), with each experiment performed in quadruplicate. (B) Orai3 knockdown was quantified using qRT-PCR at 48 h after siOrai3 delivery. Data are the mean  $\pm$  standard error of four separate experiments ( $n = 4$ ), with each experiment performed in duplicate. Cell viabilities (A) and percent Orai3 knockdowns (B) are normalized with respect to the appropriate siControl case for each formulation (shown in Figure 9). The formulations of delivery agents tested were: siRNA free in solution without the aid of any delivery agent (siOrai3), siRNA complexed with the RNAiMAX commercial transfection agent (siOrai3 + RNAiMAX), siRNA encapsulated within nonfunctionalized polymer vesicles (0% PR\_b siOrai3), and PR\_b-functionalized vesicles encapsulating siRNA (20% PR\_b siOrai3). The percentages of PR\_b functionalization

Figure 8. continued

shown are mol %. Students *t* test statistical analyses were performed, and the statistical significances were noted ( $\dagger p > 0.05$ ,  $*p < 0.05$ ,  $**p < 0.01$ ,  $***p < 0.001$ ). *P*-value markers directly above each column indicate the statistical significance between that column and the corresponding siControl case (shown in Figure 9), while markers over brackets indicate the statistical significance between the two bracketed columns.

internalizing within a cell, due to its anionic nature, and because siRNA is rapidly degraded in serum without some form of encapsulation or protection. Thus, it is unsurprising that no significant decrease in cell viability or Orai3 knockdown is observed for the case where free siOrai3 in solution was introduced to the cells (siOrai3). Without PR\_b functionalization, polymer vesicle delivery is minimal so that it could be expected that siOrai3 delivery by nonfunctionalized vesicles (0% PR\_b siOrai3) would be ineffective, as is seen in Figure 8.

In contrast, delivery of RNAiMAX complexed siOrai3 (siOrai3 + RNAiMAX) was found to be considerably more effective and gave relatively high amounts of Orai3 knockdown in both cell lines. The RNAiMAX commercial siRNA transfection agent yielded in general an average of 50–60% knockdown of Orai3 relative to the siControl case for both MCF10A cells and T47D cells, with no statistically significant difference between the knockdown levels of the two cell lines. However, a striking difference is seen in the resultant cell viability of the two cell lines for the siOrai3 + RNAiMAX case. A 37% decrease in cell viability of the T47D cancerous breast cell line as compared to the MCF10A breast cell line is observed. Just as importantly, for MCF10A cells, no statistically significant decrease in cell viability from the baseline siControl + RNAiMAX case is observed for delivery of siOrai3 by RNAiMAX. As was expected, it appears that siOrai3 is able to act as a cancer cell-specific therapeutic. It was proposed in the literature that knockdown of Orai3 could have a cancer cell-specific effect on cell viability, decreasing T47D cell viability while preserving MCF10A breast cell viability, and our results have confirmed this effect.<sup>6</sup> Considering that Orai3 was knocked down similarly for both cell lines, yet only T47D cells saw a decrease in cell viability, it is reasonable to conclude that Orai3 is critical for T47D cell proliferation and survival, while it is not for MCF10A cells, as suggested in the literature.<sup>6</sup>

Lipofectamine RNAiMAX is a well established, highly effective in vitro siRNA transfection agent. Repeated investigations have identified RNAiMAX as one of the most effective commercial siRNA transfection agents currently available.<sup>73–77</sup> Taken together, delivery of siOrai3, either complexed with RNAiMAX or as free siRNA in solution, represents an approximate window of current siRNA delivery in vitro, with RNAiMAX representing a highly effective current commercial siRNA transfection agent and free siRNA representing the least effective siRNA delivery system imaginable.

Delivery of siRNA by PR\_b-functionalized OB polymer vesicles lies within this window of delivery effectiveness. As was seen for the RNAiMAX formulation, delivery of siOrai3 encapsulated within PR\_b-functionalized polymer vesicles (20% PR\_b siOrai3) resulted in Orai3 knockdown in both cell lines, concomitant with T47D specific decreases in cell viability. However, both the amount of Orai3 knockdown and the level of T47D cell viability decrease are more moderate for

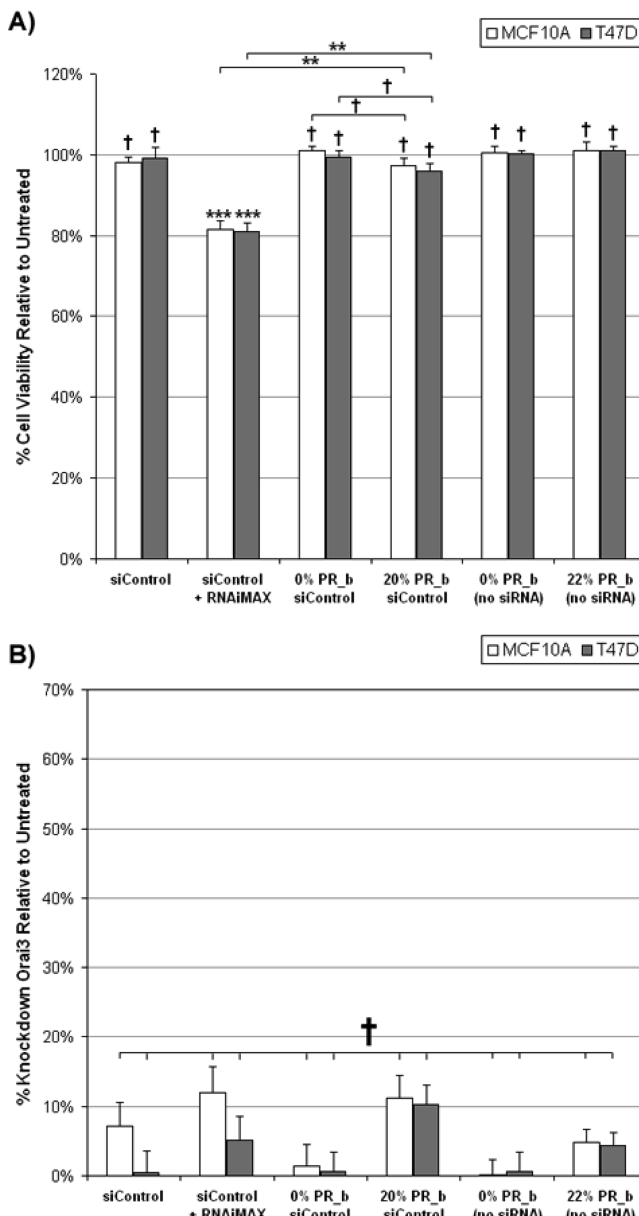


**Figure 9.** Percent cell viabilities (A) and knockdown of Orai3 (B) in MCF10A breast cells and T47D breast cancer cells after treatment with the indicated siControl formulations. Cells were incubated with 50 nM of siControl delivered as a formulation with the indicated delivery agents for 24 h at 37 °C, after which the cell medium was refreshed and incubation continued. (A) Cell viability was quantified using the MTT assay at 72 h after siControl delivery. Data are the mean  $\pm$  standard error of three separate experiments ( $n = 3$ ), with each experiment performed in quadruplicate. (B) Orai3 knockdown was quantified using qRT-PCR at 48 h after siControl delivery. Data are the mean  $\pm$  standard error of four separate experiments ( $n = 4$ ), with each experiment performed in duplicate. Cell viabilities (A) and percent Orai3 knockdowns (B) are normalized with respect to untreated cells. The formulations of delivery agents tested were: siRNA free in solution without the aid of any delivery agent (siControl), siRNA complexed with the RNAiMAX commercial transfection agent (siControl + RNAiMAX), siRNA encapsulated within nonfunctionalized polymer vesicles (0% PR<sub>b</sub> siControl), PR<sub>b</sub>-functionalized vesicles encapsulating siRNA (20% PR<sub>b</sub> siControl), and nonfunctionalized and PR<sub>b</sub>-functionalized “empty” vesicles (0% PR<sub>b</sub> and 22% PR<sub>b</sub> (no siRNA)). The percentages of PR<sub>b</sub> functionalization shown are mol %. Students *t* test statistical analyses were performed, and the statistical significances were noted as follows:  $† p > 0.05$ ,  $* p < 0.05$ ,  $** p < 0.01$ ,  $*** p < 0.001$ .

Figure 9. continued

( $† p > 0.05$ ,  $* p < 0.05$ ,  $** p < 0.01$ ,  $*** p < 0.001$ ). (A) *P*-value markers directly above each column indicate the statistical significance between that column and untreated cells, while markers over brackets indicate the statistical significance between the two bracketed columns. (B) None of the control formulations produced a statistically significantly difference ( $p > 0.05$  for all) in siOrai3 expression as compared to the untreated cells, as indicated by the overarching all-inclusive bracket.

the case of siOrai3 delivery by PR<sub>b</sub>-functionalized OB polymer vesicles as compared to the delivery by RNAiMAX, suggesting that only a portion of the siRNA may have escaped from the nondegradable OB block copolymer vesicles. Still, siOrai3 delivery by PR<sub>b</sub>-functionalized polymer vesicles effects on average 22% knockdown of Orai3 expression and a 22% decrease in T47D cell viability, relative to siControl baselines. Just as with the RNAiMAX case, no measurable drop in cell viability is elicited in the breast cell line, MCF10A. Although these results are not overwhelmingly positive for siRNA delivery by the polymer vesicles, one must keep in mind that these are for a model OB block (nondegradable) copolymer system and they can represent a first step toward future improvements and advancements in polymersome design tailored for the task of siRNA delivery.

Figure 9 shows the percent cell viabilities and Orai3 knockdowns relative to untreated cells for each of the control cases, both siControl formulated with varying delivery agents and “empty” polymer vesicles containing no siRNA. First, it must be pointed out than none of the control cases produced a statistically significant knockdown in Orai3 expression (Figure 9B) as compared to the untreated cells as indicated by the overarching all-inclusive bracket in this figure. This is unsurprising given that siControl is designed to give minimal off-target knockdown of gene expression, and certainly no Orai3 knockdown could be expected for “empty” polymer vesicles, because no siRNA is delivered. Likewise, for all of the control formulations except the RNAiMAX transfection agent (siControl + RNAiMAX), no statistically significant decrease in cell viability is observed as compared to the untreated cells (Figure 9A). Corroborating previous reports in the literature concerning the biocompatibility and nontoxic nature of OB polymer vesicles, “empty” polymer vesicles, both nonfunctionalized (0% PR<sub>b</sub> (no siRNA)) and PR<sub>b</sub>-functionalized (22% PR<sub>b</sub> (no siRNA)), were found to have no effect on the cell viability of either cell line.<sup>27,28,43</sup> In addition, encapsulation and delivery of control siRNA by polymer vesicles (0% PR<sub>b</sub> siControl and 20% PR<sub>b</sub> siControl) also were found to have no statistically significant effect on cell viability as compared to the untreated cells. In Figure 8B it was seen that PR<sub>b</sub>-functionalized polymer vesicles are capable of delivering siRNA at moderate levels so that it is likely that siControl is being delivered to the cells for this case in Figure 9 as well. The levels of siControl delivered to cells by PR<sub>b</sub>-functionalized polymer vesicles appear then to have no significant effect on the viability of either cell line.

In contrast to all of the other control cases shown in Figure 9A, the RNAiMAX transfection agent complexed with siControl (siControl + RNAiMAX) produced an approximately 19% drop in cell viability for both MCF10A noncancerous breast cells and T47D breast cancer cells. It is unclear from these data whether this decrease in cell viability derives from the RNAiMAX transfection agent itself or from the delivery of

siControl, or as is more likely a combination of the two. It should be noted that others have observed similar levels of toxicity for the RNAiMAX transfection agent, and in fact among the variety of commercial siRNA transfection agents currently available, RNAiMAX is recognized as one of the least toxic and most effective.<sup>73–79</sup> Figure 9A clearly shows that RNAiMAX complexed with siControl (siControl + RNAiMAX) gives some moderate toxicity in both cell lines as compared to both untreated cells and delivery of siControl by PR\_b-functionalized polymersomes (20% PR\_b siControl). However, it is uncertain to what extent this difference in toxicity derives from the differing levels of actual siRNA delivery from these two formulations, considering that Figure 8 indicates that not all of the siRNA can escape from the nondegradable OB polymersomes. Ideally, one would like to measure the cell viabilities resulting from RNAiMAX delivered alone without siRNA to assess the inherent toxicity of the delivery agent itself, similar to what was done with “empty” polymer vesicles. This experiment was attempted; however, an accurate measure of the toxicity of RNAiMAX alone could not be obtained. Because the RNAiMAX transfection agent forms a complex with siRNA in solution, and it is this tightly bound complex that delivers to the cells, delivery of the RNAiMAX reagent alone (i.e., uncomplexed, without any siRNA) is inherently different and does not interact with cells in a similar manner, and thus does not represent a valid measure of the RNAiMAX toxicity.

## CONCLUSION

In this study, we investigated the ability of peptide-functionalized OB polymer vesicles to deliver siRNA to T47D breast cancer cells and compared this delivery to that with MCF10A breast cells. Both GRGDSP and PR\_b peptide-functionalized polymer vesicles were found to effectively deliver to both cell lines; however, PR\_b-functionalized vesicles gave significantly higher levels of delivery. In addition, PR\_b functionalization of polymer vesicles resulted in significantly more delivery of encapsulates to cancerous T47D cells as compared to MCF10A cells. Confocal microscopy with endosomal and lysosomal intracellular organelles stained for visualization of colocalization revealed that PR\_b polymer vesicles, upon internalization, are passed through the endosomes and lysosomes. The polymer vesicle encapsulate was most colocalized with early endosomes, and it was also found that the majority of encapsulate release from polymer vesicles occurs in the early endosomes. Also, the data may suggest some evidence of organelle escape. siRNA molecules were then effectively encapsulated within polymer vesicles and delivered to these cell lines. The Orai3 gene was targeted for siRNA knockdown, because a recent report in the literature indicated that knockdown of Orai3 could have a differential effect on cell viability for breast cancer cells, as opposed to noncancerous breast cells.<sup>6</sup> Delivery of siRNA targeting the Orai3 gene, siOrai3, by PR\_b-functionalized polymer vesicles gave Orai3 knockdown in both cell lines, but decreased T47D, breast cancer cell viability, while having no measurable negative effect on the viability of MCF10A breast cells. As compared to the highly effective commercial transfection agent, Lipofectamine RNAiMAX, Orai3 knockdown by PR\_b-functionalized OB polymer vesicles is admittedly moderate; however, lower toxicity was observed for the delivery of siRNA by polymer vesicles as opposed to by RNAiMAX. Although both encapsulate release from the nondegradable polymer vesicles and some encapsulate escape

from acidic organelles was observed, neither was highly prevalent. These factors likely contribute to the only moderate levels of Orai3 knockdown observed for PR\_b-functionalized OB vesicles, even though these vesicles were found to be very effectively internalized by the cells. However, the results shown here are promising, considering that these OB polymer vesicles are a first generation model nondegradable polymer vesicle system. Future improvements could likely be achieved for siRNA delivery by polymer vesicles by designing block copolymers that would more effectively release encapsulates and facilitate endosomal escape.

## AUTHOR INFORMATION

### Corresponding Author

\*Phone: (612) 626-1185. Fax: (612) 626-7246. E-mail: kokkoli@umn.edu.

### Notes

The authors declare no competing financial interest.

## ACKNOWLEDGMENTS

This work was supported in part by the Camille Dreyfus Teacher-Scholar Awards Program.

## REFERENCES

- (1) Fire, A.; Xu, S.; Montgomery, M. K.; Kostas, S. A.; Driver, S. E.; Mello, C. C. Potent and specific genetic interference by double-stranded RNA in *Caenorhabditis elegans*. *Nature* **1998**, *391*, 806–11.
- (2) Dorsett, Y.; Tuschl, T. siRNAs: applications in functional genomics and potential as therapeutics. *Nat. Rev. Drug Discovery* **2004**, *3*, 318–29.
- (3) Hamilton, A. J. A species of small antisense RNA in posttranscriptional gene silencing in plants. *Science* **1999**, *286*, 950–952.
- (4) Carthew, R. W.; Sontheimer, E. J. Origins and mechanisms of miRNAs and siRNAs. *Cell* **2009**, *136*, 642–55.
- (5) Pai, S. I.; Lin, Y.-Y.; Macaes, B.; Meneshian, A.; Hung, C.-F.; Wu, T.-C. Prospects of RNA interference therapy for cancer. *Gene Ther.* **2006**, *13*, 464–77.
- (6) Faouzi, M.; Hague, F.; Potier, M.; Ahidouch, A.; Sevestre, H.; Ouadid-Ahidouch, H. Down-regulation of Orai3 arrests cell-cycle progression and induces apoptosis in breast cancer cells but not in normal breast epithelial cells. *J. Cell. Physiol.* **2010**, *226*, 542–551.
- (7) Roberts-Thomson, S. J.; Peters, A. A.; Grice, D. M.; Monteith, G. R. ORAI-mediated calcium entry: Mechanism and roles, diseases and pharmacology. *Pharmacol. Ther.* **2010**, *127*, 121–130.
- (8) Gwack, Y.; Srikanth, S.; Feske, S.; Cruz-Guilloty, F.; Oh-hora, M.; Neems, D. S.; Hogan, P. G.; Rao, A. Biochemical and functional characterization of Orai proteins. *J. Biol. Chem.* **2007**, *282*, 16232–16243.
- (9) Potier, M.; Gonzalez, J. C.; Motiani, R. K.; Abdullaev, I. F.; Bisailon, J. M.; Singer, H. A.; Trebak, M. Evidence for STIM1- and Orai1-dependent store-operated calcium influx through ICRAC in vascular smooth muscle cells: role in proliferation and migration. *FASEB J.* **2009**, *23*, 2425–2437.
- (10) Kahl, C. R.; Means, A. R. Regulation of cell cycle progression by calcium/calmodulin-dependent pathways. *Endocr. Rev.* **2003**, *24*, 719–736.
- (11) Taylor, J. T.; Zeng, X.-B.; Pottle, J. E.; Lee, K.; Wang, A. R.; Yi, S. G.; Scruggs, J. A. S.; Sikka, S. S.; Li, M. Calcium signaling and T-type calcium channels in cancer cell cycling. *World J. Gastroenterol.* **2008**, *14*, 4984–91.
- (12) Motiani, R. K.; Abdullaev, I. F.; Trebak, M. A novel native store-operated calcium channel encoded by Orai3: selective requirement of Orai3 versus Orai1 in estrogen receptor-positive versus estrogen receptor-negative breast cancer cells. *J. Biol. Chem.* **2010**, *285*, 19173–19183.

- (13) Strobl, J. S.; Wonderlin, W. F.; Flynn, D. C. Mitogenic signal transduction in human breast cancer cells. *Gen. Pharmacol.* **1995**, *26*, 1643–9.
- (14) Yang, S.; Zhang, J. J.; Huang, X.-Y. Orai1 and STIM1 are critical for breast tumor cell migration and metastasis. *Cancer Cell* **2009**, *15*, 124–134.
- (15) Mignen, O.; Thompson, J. L.; Shuttleworth, T. J. Both Orai1 and Orai3 are essential components of the arachidonate-regulated Ca<sup>2+</sup>-selective (ARC) channels. *J. Physiol.* **2008**, *586*, 185–95.
- (16) Masiero, M.; Nardo, G.; Indraccolo, S.; Favaro, E. RNA interference: implications for cancer treatment. *Mol. Aspects Med.* **2007**, *28*, 143–66.
- (17) Whitehead, K. A.; Langer, R.; Anderson, D. G. Knocking down barriers: advances in siRNA delivery. *Nat. Rev. Drug Discovery* **2009**, *8*, 129–38.
- (18) Lechner, M. C.; Duque Magalhães, M. C. RNase activities in blood serum of several vertebrates. *Experientia* **1973**, *29*, 1479–1480.
- (19) Kurreck, J. Antisense technologies. Improvement through novel chemical modifications. *Eur. J. Biochem.* **2003**, *270*, 1628–1644.
- (20) Discher, D. E.; Ortiz, V.; Srinivas, G.; Klein, M. L.; Kim, Y.; Christian, D.; Cai, S.; Photos, P.; Ahmed, F. Emerging applications of polymersomes in delivery: From molecular dynamics to shrinkage of tumors. *Prog. Polym. Sci.* **2007**, *32*, 838–857.
- (21) Discher, D. E.; Ahmed, F. Polymersomes. *Annu. Rev. Biomed. Eng.* **2006**, *8*, 323–341.
- (22) Kita-Tokarczyk, K.; Grumelard, J.; Haefele, T.; Meier, W. Block copolymer vesicles—using concepts from polymer chemistry to mimic biomembranes. *Polymer* **2005**, *46*, 3540–3563.
- (23) Battaglia, G.; Ryan, A. J. Bilayers and interdigitation in block copolymer vesicles. *J. Am. Chem. Soc.* **2005**, *127*, 8757–8764.
- (24) Mintzer, M. A.; Simanek, E. E. Nonviral vectors for gene delivery. *Chem. Rev.* **2009**, *109*, 259–302.
- (25) Christian, D. A.; Cai, S.; Bowen, D. M.; Kim, Y.; Pajerowski, J. D.; Discher, D. E. Polymersome carriers: From self-assembly to siRNA and protein therapeutics. *Eur. J. Pharm. Biopharm.* **2009**, *71*, 463–474.
- (26) Napper, D. H. Steric stabilization. *J. Colloid Interface Sci.* **1977**, *58*, 390–407.
- (27) Photos, P. J.; Bacakova, L.; Discher, B.; Bates, F. S.; Discher, D. E. Polymer vesicles in vivo: correlations with PEG molecular weight. *J. Controlled Release* **2003**, *90*, 323–334.
- (28) Pangburn, T. O.; Bates, F. S.; Kokkoli, E. Polymersomes functionalized via “click” chemistry with the fibronectin mimetic peptides PR\_b and GRGDSP for targeted delivery to cells with different levels of  $\alpha_5\beta_1$  expression. *Soft Matter* **2012**, *8*, 4449–4461.
- (29) Mardilovich, A.; Craig, J. A.; McCammon, M. Q.; Garg, A.; Kokkoli, E. Design of a novel fibronectin-mimetic peptide-amphiphile for functionalized biomaterials. *Langmuir* **2006**, *22*, 3259–3264.
- (30) Craig, J. A.; Rexeisen, E. L.; Mardilovich, A.; Shroff, K.; Kokkoli, E. Effect of linker and spacer on the design of a fibronectin mimetic peptide evaluated via cell studies and AFM adhesion forces. *Langmuir* **2008**, *24*, 10282–10292.
- (31) Mardilovich, A.; Kokkoli, E. Biornimetic peptide-amphiphiles for functional biomaterials: The role of GRGDSP and PHSRN. *Biomacromolecules* **2004**, *5*, 950–957.
- (32) Aota, S.; Nomizu, M.; Yamada, K. M. The short amino acid sequence Pro-His-Ser-Arg-Asn in human fibronectin enhances cell-adhesive function. *J. Biol. Chem.* **1994**, *269*, 24756–24761.
- (33) Garcia, A. J.; Schwarzbauer, J. E.; Boettiger, D. Distinct activation states of  $\alpha_5\beta_1$  integrin show differential binding to RGD and synergy domains of fibronectin. *Biochemistry* **2002**, *41*, 9063–9069.
- (34) Kokkoli, E.; Ochsenhirt, S. E.; Tirrell, M. Collective and single-molecule interactions of  $\alpha_5\beta_1$  integrins. *Langmuir* **2004**, *20*, 2397–2404.
- (35) Garg, A.; Tisdale, A. W.; Haidari, E.; Kokkoli, E. Targeting colon cancer cells using PEGylated liposomes modified with a fibronectin-mimetic peptide. *Int. J. Pharm.* **2009**, *366*, 201–210.
- (36) Demirgöz, D.; Garg, A.; Kokkoli, E. PR\_b targeted PEGylated liposomes for prostate cancer therapy. *Langmuir* **2008**, *24*, 13518–13524.
- (37) Demirgöz, D.; Pangburn, T. O.; Davis, K. P.; Lee, S.; Bates, F. S.; Kokkoli, E. PR\_b-targeted delivery of tumor necrosis factor-a by polymersomes for the treatment of prostate cancer. *Soft Matter* **2009**, *5*, 2011–2019.
- (38) Fernandez-Cobo, M.; Holland, J. F.; Pogo, B. G. T. Transcription profiles of non-immortalized breast cancer cell lines. *BMC Cancer* **2006**, *6*, 99.
- (39) Saad, S.; Bendall, L. J.; James, A.; Gottlieb, D. J.; Bradstock, K. F. Induction of matrix metalloproteinases MMP-1 and MMP-2 by co-culture of breast cancer cells and bone marrow fibroblasts. *Breast Cancer Res. Treat.* **2000**, *63*, 105–115.
- (40) Jia, Y.; Zeng, Z.-Z.; Markwart, S. M.; Rockwood, K. F.; Ignatoski, K. M. W.; Ethier, S. P.; Livant, D. L. Integrin fibronectin receptors in matrix metalloproteinase-1-dependent invasion by breast cancer and mammary epithelial cells. *Cancer Res.* **2004**, *64*, 8674–8681.
- (41) van der Pluijm, G.; Vloedgraven, H.; Papapoulos, S.; Löwick, C.; Grzesik, W.; Kerr, J.; Robey, P. G. Attachment characteristics and involvement of integrins in adhesion of breast cancer cell lines to extracellular bone matrix components. *Lab. Invest.* **1997**, *77*, 665–75.
- (42) Hillmyer, M. A.; Bates, F. S. Synthesis and characterization of model polyalkane-poly(ethylene oxide) block copolymers. *Macromolecules* **1996**, *29*, 6994–7002.
- (43) Lee, J. C.-M.; Bermudez, H.; Discher, B. M.; Sheehan, M. A.; Won, Y.-Y.; Bates, F. S.; Discher, D. E. Preparation, stability, and in vitro performance of vesicles made with diblock copolymers. *Biotechnol. Bioeng.* **2001**, *73*, 135–145.
- (44) Rostovtsev, V. V.; Green, L. G.; Fokin, V. V.; Sharpless, K. B. A stepwise Huisgen cycloaddition process: Copper(I)-catalyzed regioselective “ligation” of azides and terminal alkynes. *Angew. Chem., Int. Ed.* **2002**, *41*, 2596–2599.
- (45) Lewis, W. G.; Magallon, F. G.; Fokin, V. V.; Finn, M. G. Discovery and characterization of catalysts for azide-alkyne cycloaddition by fluorescence quenching. *J. Am. Chem. Soc.* **2004**, *126*, 9152–9153.
- (46) Gupta, S. S.; Kuzelka, J.; Singh, P.; Lewis, W. G.; Manchester, M.; Finn, M. G. Accelerated bioorthogonal conjugation: A practical method for the ligation of diverse functional molecules to a polyvalent virus scaffold. *Bioconjugate Chem.* **2005**, *16*, 1572–1579.
- (47) Rodionov, V. O.; Presolski, S. I.; Gardinier, S.; Lim, Y. H.; Finn, M. G. Benzimidazole and related ligands for Cu-catalyzed azide-alkyne cycloaddition. *J. Am. Chem. Soc.* **2007**, *129*, 12696–12704.
- (48) Pata, V.; Ahmed, F.; Discher, D. E.; Dan, N. Membrane solubilization by detergent: Resistance conferred by thickness. *Langmuir* **2004**, *20*, 3888–3893.
- (49) Abramoff, M. D.; Magalhaes, P. J.; Ram, S. J. Image processing with ImageJ. *Biophotonics Int.* **2004**, *11*, 36–42.
- (50) Costes, S. V.; Daelemans, D.; Cho, E. H.; Dobbin, Z.; Pavlakis, G.; Lockett, S. Automatic and quantitative measurement of protein-protein colocalization in live cells. *Biophys. J.* **2004**, *86*, 3993–4003.
- (51) Livak, K. J.; Schmittgen, T. D. Analysis of relative gene expression data using real-time quantitative PCR and the 2(-Delta Delta C(T)) method. *Methods* **2001**, *25*, 402–8.
- (52) Vandesompele, J.; De Preter, K.; Pattyn, F.; Poppe, B.; Van Roy, N.; De Paepe, A.; Speleman, F. Accurate normalization of real-time quantitative RT-PCR data by geometric averaging of multiple internal control genes. *Genome Biol.* **2002**, *3*, research0034.1–research0034.11.
- (53) Jain, S.; Bates, F. S. On the origins of morphological complexity in block copolymer surfactants. *Science* **2003**, *300*, 460–464.
- (54) Jain, S.; Dyrdahl, M. H. E.; Gong, X.; Scriven, L. E.; Bates, F. S. Lyotropic phase behavior of poly(ethylene oxide)-poly(butadiene) diblock copolymers: Evolution of the random network morphology. *Macromolecules* **2008**, *41*, 3305–3316.
- (55) Jain, S.; Bates, F. S. Consequences of nonergodicity in aqueous binary PEO-PB micellar dispersions. *Macromolecules* **2004**, *37*, 1511–1523.
- (56) Discher, B. M.; Won, Y. Y.; Ege, D. S.; Lee, J. C. M.; Bates, F. S.; Discher, D. E.; Hammer, D. A. Polymersomes: Tough vesicles made from diblock copolymers. *Science* **1999**, *284*, 1143–1146.

- (57) Won, Y. Y.; Davis, H. T.; Bates, F. S. Molecular exchange in PEO-PB micelles in water. *Macromolecules* **2003**, *36*, 953–955.
- (58) Iyer, A. K.; Khaled, G.; Fang, J.; Maeda, H. Exploiting the enhanced permeability and retention effect for tumor targeting. *Drug Discovery Today* **2006**, *11*, 812–818.
- (59) Opsteen, J. A.; Brinkhuis, R. P.; Teeuwen, R. L. M.; Lowik, D. W. P. M.; van Hest, J. C. M. “Clickable” polymersomes. *Chem. Commun.* **2007**, 3136–3138.
- (60) Wang, X.; Liu, L.; Luo, Y.; Zhao, H. Bioconjugation of biotin to the interfaces of polymeric micelles via in situ click chemistry. *Langmuir* **2009**, *25*, 744–750.
- (61) Pakalns, T.; Haverstick, K.; Fields, G. B.; McCarthy, J. B.; Mooradian, D.; Tirrell, M. Cellular recognition of synthetic peptide amphiphiles in self-assembled monolayer films. *Biomaterials* **1999**, *20*, 2265–2279.
- (62) Flatin, G. E.; Dhanikula, A. B.; Luthman, K.; Brandl, M. Drug permeability across a phospholipid vesicle based barrier: A novel approach for studying passive diffusion. *Eur. J. Pharm. Sci.* **2006**, *27*, 80–90.
- (63) Kim, Y.; Tewari, M.; Pajerowski, J. D.; Cai, S.; Sen, S.; Williams, J.; Sirsi, S.; Lutz, G.; Discher, D. E. Polymersome delivery of siRNA and antisense oligonucleotides. *J. Controlled Release* **2009**, *134*, 132–140.
- (64) Auguste, D. T.; Furman, K.; Wong, A.; Fuller, J.; Armes, S. P.; Deming, T. J.; Langer, R. Triggered release of siRNA from poly(ethylene glycol)-protected, pH-dependent liposomes. *J. Controlled Release* **2008**, *130*, 266–274.
- (65) Mei, J.; Hu, H.; McEntee, M.; Plummer, H., III; Song, P.; Wang, H.-C. R. Transformation of non-cancerous human breast epithelial cell line MCF10A by the tobacco-specific carcinogen NNK. *Breast Cancer Res. Treat.* **2003**, *79*, 95–105.
- (66) Garg, A.; Kokkoli, E. pH-Sensitive PEGylated liposomes functionalized with a fibronectin-mimetic peptide show enhanced intracellular delivery to colon cancer cells. *Curr. Pharm. Biotechnol.* **2011**, *12*, 1135–1143.
- (67) Woodle, M. C.; Lasic, D. D. Sterically stabilized liposomes. *Biochim. Biophys. Acta, Rev. Biomembr.* **1992**, *1113*, 171–199.
- (68) Ahmed, F.; Pakunlu, R. I.; Srinivas, G.; Brannan, A.; Bates, F.; Klein, M. L.; Minko, T.; Discher, D. E. Shrinkage of a rapidly growing tumor by drug-loaded polymersomes: pH-Triggered release through copolymer degradation. *Mol. Pharmaceutics* **2006**, *3*, 340–350.
- (69) Plopper, G. E.; Domanico, S. Z.; Cirulli, V.; Kiosses, W. B.; Quaranta, V. Migration of breast epithelial cells on Laminin-5: differential role of integrins in normal and transformed cell types. *Breast Cancer Res. Treat.* **1998**, *51*, 57–69.
- (70) Dunehoo, A. L.; Anderson, M.; Majumdar, S.; Kobayashi, N.; Berkland, C.; Siahaan, T. J. Cell adhesion molecules for targeted drug delivery. *J. Pharm. Sci.* **2006**, *95*, 1856–1872.
- (71) Bohley, P.; Seglen, P. Proteases and proteolysis in the lysosome. *Experientia* **1992**, *48*, 151–157.
- (72) Noh, S. M.; Han, S. E.; Shim, G.; Lee, K. E.; Kim, C.-W.; Han, S. S.; Choi, Y.; Kim, Y. K.; Kim, W.-K.; Oh, Y.-K. Tocopheryl oligochitosan-based self assembling oligomersomes for siRNA delivery. *Biomaterials* **2011**, *32*, 849–57.
- (73) Zhao, M.; Yang, H.; Jiang, X.; Zhou, W.; Zhu, B.; Zeng, Y.; Yao, K.; Ren, C. Lipofectamine RNAiMAX: an efficient siRNA transfection reagent in human embryonic stem cells. *Mol. Biotechnol.* **2008**, *40*, 19–26.
- (74) Carralot, J.-P.; Kim, T.-K.; Lenseigne, B.; Boese, A. S.; Sommer, P.; Genovesio, A.; Brodin, P. Automated high-throughput siRNA transfection in raw 264.7 macrophages: a case study for optimization procedure. *J. Biomol. Screening* **2009**, *14*, 151–60.
- (75) Pawłowski, K. M.; Popielarz, D.; Szyszko, K.; Gajewska, M.; Motyl, T.; Król, M. Growth hormone receptor (ghr) RNAi decreases proliferation and enhances apoptosis in CMT-U27 canine mammary carcinoma cell line. *Vet. Comp. Oncol.* **2012**, *10*, 2–15.
- (76) Nabzdyk, C. S.; Chun, M.; Pradhan, L.; Logerfo, F. W. High throughput RNAi assay optimization using adherent cell cytometry. *J. Transl. Med.* **2011**, *9*, 48.
- (77) Brough, R.; Frankum, J. R.; Sims, D.; Mackay, A.; Mendes-Pereira, A. M.; Bajrami, I.; Costa-Cabral, S.; Rafiq, R.; Ahmad, A. S.; Cerone, M. A.; Natrajan, R.; Sharpe, R.; Shiu, K.-K.; Wetterskog, D.; Dedes, K. J.; Lambros, M. B.; Rawjee, T.; Linardopoulos, S.; Reis-Filho, J. S.; Turner, N. C.; Lord, C. J.; Ashworth, A. Functional viability profiles of breast cancer. *Cancer Discovery* **2011**, *1*, 260–273.
- (78) Breunig, M.; Hozsa, C.; Lungwitz, U.; Watanabe, K.; Umeda, I.; Kato, H.; Goepfertich, A. Mechanistic investigation of poly(ethylene imine)-based siRNA delivery: Disulfide bonds boost intracellular release of the cargo. *J. Controlled Release* **2008**, *130*, 57–63.
- (79) Suhorutsenko, J.; Oskolkov, N.; Arukuusk, P.; Kurrikoff, K.; Eriste, E.; Copolovici, D.-M.; Langel, U. Cell-penetrating peptides, PepFects, show no evidence of toxicity and immunogenicity in vitro and in vivo. *Bioconjugate Chem.* **2011**, *22*, 2255–62.